Integrated microfossil biostratigraphy, facies distribution and depositional sequences of the upper Turonian to Campanian succession in northeast Egypt and Jordan

Sherif Farouk*, Fayez Ahmad, John H. Powell, Akmal M. Marzouk

Sherif Farouk*
Exploration Department, Egyptian Petroleum Research Institute, Nasr City, 11727, Egypt
e-mail: geo.sherif@hotmail.com
Fayez Ahmad
Earth and Environmental sciences Department, Hashemite University, Jordan
John H. Powell
British Geological Survey, Nottingham, UK
Akmal M. Marzouk
Geology Department, Faculty of Science, Tanta University, Egypt

Abstract Six upper Turonian to Campanian sections in Egypt (Sinai) and Jordan were studied for their microfossil biostratigraphy (calcareous nannofossils and planktonic foraminifera), facies distribution and sequence stratigraphic frameworks. Carbonate (mostly chalk) and chert lithofacies dominate the basinward northern sections passing laterally and vertically to mixed carbonate/siliciclastic lithofacies towards the shoreline in the southeast. Twenty-six lithofacies types have been identified and grouped into six lithofacies associations: littoral siliciclastic facies belt; peritidal carbonate; intertidal carbonate platform/ramp; high-energy ooidal shoals and shelly biostromes; shallow subtidal; and pelagic facies association. The following calcareous nannofossil biozones were recognized: *Luianorhabdus malefomis* (CC12) (late Turonian), *Micula staurophora* (CC14) (early Coniacian), *Reinhardtites anthophorus* (CC15) (late Coniacian), *Lucianorhabdus cayeuxii* (CC16) (early Santonian) and *Broinsonia* *parca parca* (CC18) (Campanian). Equivalent planktonic foraminifera zones recognized are: *Dicarinella concavata* (Coniacian), the lower most part of *D. asymetrica* (earliest Santonian) and *Globotruncanita elevata* (early Campanian). The integrated zonation presented here is considered to provide higher resolution than the use of either group alone. The absence of calcareous nannofossil biozones CC13 and CC17 in most of the studied sections, associated with regional vertical lithofacies changes, indicates that recognition of the Turonian/Coniacian and Santonian/Campanian stage boundary intervals in the region have been hampered by depositional hiatuses at major sequence boundaries resulting in incomplete sections. These disconformities are attributed to eustatic sea-level fluctuations and regional tectonics resulting from flexuring of the Syrian Arc fold belt. The Coniacian to Santonian succession can be divided into three third-order depositional sequences which are bounded by four widely recognized sequence boundaries.

Keywords: Planktonic biostratigraphy, late Turonian, Coniacian, Santonian, Campanian**,** sequence stratigraphy, Arabian platform, Jordan, Egypt.

Introduction

Upper Cretaceous successions are widely distributed and well-exposed in north Egypt (Sinai) Jordan, Israel and the Levant, an area that formed the northeastern part of the Arabian Platform. These successions are characterized by marked lateral and vertical changes in lithofacies resulting from the interplay of eustatic sea-level fluctuations and the influence of regional intra-plate tectonics (Krenkel 1924; Reiss et al. 1985; Gvirtzman et al. 1985; Powell 1989; Lüning et al. 1998a-b; Soudry et al. 2006). Biostratigraphical analyses of the Turonian/Coniacian, Coniacian/Santonian and Santonian/Campanian stage boundary successions in the region have been hampered by periods of depositional hiatus resulting in incomplete sections and/or hardgrounds (e.g. Lewy 1990; Gruszczynski et al. 2002; Powell and Moh'd 2012; Farouk and Faris 2012; Meilijson 2014).

Numerous studies have been published on the facies analysis and reconstruction of depositional environments of the Coniacian to Campanian successions (e.g. Koch 1968; Lewy 1990; Almogi-Labin et al. 1993; Kuss 1986; Powell 1988, 1989; Cherif and Ismail 1991; Kora and Genedi 1995; Lüning et al. 1998a-b; Moh'd 2000; Mustafa 2000; Mustafa et al. 2002; Kuss et al. 2000; Bauer et al. 2002, 2003; Abdel-Gawad et al. 2004; El-Azabi and El-Araby 2007; Shahin and Kora 1991; Issawi et al. 2009; Powell and Moh`d 2011, 2012; Ismail 2012; Makhlouf et al. 2015 and Farouk 2015). The precise correlation of the upper Turonian to Campanian successions in Egypt, Jordan and Israel on a regional scale, based upon integrated litho- and biostratigraphy, and the distribution of lithofacies tracts has, to date, been uncertain. Furthermore, comparison and correlation of the sequences in this region to global (eustatic) sea-level events (Haq, 2014) is controversial as a result of regional (eurybatic) fluctuations on the Arabian Platform that were influenced by Late Cretaceous tectonic deformation of the Syrian Arc (Krenkel 1924; Soudry et al. 1985; Flexer et al. 1986; Shahar 1994; Lüning et al. 1998; Meilijson et al. 2014).

Regional correlation of sequence boundaries based upon biostratigraphy provides important information on relative sea-level fluctuations on the southern margin of Neo-Tethys. These data help to elucidate the effect of local tectonics on the development of depositional sequences that can be more widely correlated with the global cycle charts (Hardenbol et al. 1998; Stampfli and Borel 2002; Haq and Al-Qahtani 2005; Haq 2014).

The aims of this paper are to: (1) determine the lithofacies characteristics and biostratigraphic framework of the upper Turonian to Campanian sequences and their palaeoenvironments, (2) establish a standard sequence stratigraphic scheme, and compare its depositional sequences and boundaries with those previously published, (3) re-evaluate the nature, extent and hiatus of the recorded sequence boundaries, (4) improve correlation with sequence boundaries recognized elsewhere in North Africa, the Arabian Platform, Europe, and with global records, (5) constrain better the timing of sea-level variations, and (6) reconstruct, precisely, the depositional history in the region during late Turonian to Santonian time.

Geological setting

In Mesozoic times, Egypt, Jordan and Israel were situated at the southern margin of the Neo-Tethys Ocean (Stampfli and Borel 2002; Ahmad et al. 2014; Meilijson et al. 2014). Many dramatic lateral and vertical lithofacies changes are observed during the convergence of the African-Arabian Craton (closure of Neo-Tethys) that resulted in the variable development of basins and swells in the region in response to the major intra-plate tectonic pulse of the 'Syrian Arc' fold belt (Krenkel 1924; Bowen and Jux 1987; Shahar 1994). At the end of the Turonian, a phase of non-deposition or local uplift and erosion, respectively, lasted until the early Coniacian (Flexer et al. 1986; Gvirtzman et al. 1989; Powell 1989; Powell and Moh'd 2011). This event is attributed to tectonic (intra-plate) foundering, subsidence and tilting of the platform margin, possibly linked to ophiolite obduction in northeast Arabia (Haq and Al-Qahtani 2005), and is also associated with extensional rifting in the Azraq Basin (Powell and Moh'd 2011). During the Coniacian a global sea-level rise (Haq 2014) resulted in marine transgression (marine flooding) across the pre-existing, rimmed carbonate platform. Transgressive marine flooding was characterized by chalk sedimentation with regressive events characterized by a marl-chert-phosphorite association; these lithofacies associations passed shorewards (southeast) to shallow marine carbonates/siliciclastics in Jordan and Egypt (Powell and Moh'd 2011).

Regional variations in the lithofacies and associated fauna and nannoflora are observed during Coniacian-Santonian time, ranging from predominantly carbonate ramp lithofacies in basinward settings towards the north and northwest (Wadi Umm Ghudran and Themed formations), to mixed shallow-water clastic/carbonate facies (Alia and Matulla formations) towards the southeast and south, depending on their relative palaeogeographic and tectonic setting. The Campanian (and Maastrichtian) sea in this region was characterized by a high concentration of organic material deposited in a broad, shallow-water zone locally associated with oyster bioherms, which led to the accumulation of economic phosphate deposits in Jordan (Powell 1989). Elevated levels of organic matter and the deposition of phosphate and organic-rich carbonates (Abed et al. 2005) at discrete levels within this succession was the result of high oceanic bio-productivity and upwelling of nutrients at the shelf margin (Almogi-Labin et al. 1993; Soudry et al. 2006; Abed et al 2007; Powell and Moh'd 2011; Meilijson et al. 2014). In contrast, the observed basinal facies in north Egypt are represented by hemiplegic facies of the Sudr Chalk Formation in north Eastern Desert/Sinai and the equivalent Khoman Chalk Formation in the Western Desert. These hemipelagic chalk facies pass laterally to mixed siliciclastic/carbonate lithofacies of the Dakhla Formation, which was deposited close to the shoreline in central and southern Egypt.

Material and Methods

Lithostratigraphical, biostratigraphical and sedimentological investigations were carried out on six exposed sections in north eastern Egypt and Jordan (Fig. 1); a total of 227 samples were collected. The sections, measured and sampled bed-by-bed, are located from south to north: Gebel Qabaliat (28º20'25"N; 33º31'36"E) and Gebel Nazazat (28º47'45"N; 33º13'19"E) in southwestern Sinai and Ras el-Gifa section in west-central Sinai (32º34'15"N; 35º48'44"E). In Jordan, sections were measured at Karak (31º02'17"N; 35º34'55"E) and Wadi Mujib (31º27'13"N; 35º48'02"E) in central Jordan, and at Wadi El-Ghafar in north Jordan (32º34'15"N; 35º48'44"E). The facies analysis of the Coniacian-Santonian successions is based on an integrated study of litho- and bio-facies in addition to a microfacies study of 160 thin-sections. The sandstones are described following the classification of Pettijohn et al. (1987), while the classification scheme of Dunham (1962), with the modifications by Embry and Klovan (1972), is used to describe the microfacies of the carbonate rocks. In addition, whole samples were examined for their calcareous nannofossil and planktonic foraminifera taxa to provide an improved biostratigraphical correlation between Egypt, Jordan, Israel and farther afield. For the foraminiferal analyses, about 20 g of dry rock were soaked in hydrogen peroxide, disaggregated in water, washed through a 63 µm sieve, and then dried. The most important foraminiferal specimens were digitally imaged under the Phillips XL30 Scanning Electron Microscope (SEM) in the laboratories of the Egyptian Mineral Resources Authority (E.M.R.A.), having been sputter-coated for 8 min with gold at 20–30 mA°. Calcareous nannofossils were studied following the method of Bramlette and Sullivan (1961) and Hay (1965).

Lithostratigraphy

The Coniacian-Santonian succession in north eastern Egypt and Jordan comprises four rock units, from north to south: Wadi Umm Ghudran and Alia Sandstone formations (Jordan) and Themed and Matulla formations (Egypt/Sinai) (Figs. 1- 5 and 6A-B). These are described below, from older to younger (Figs. 3, 4 and 5). The abbreviations Jo (Jordan) and Eg/S (Egypt /Sinai) are used to distinguish the location of these units.

Wadi Umm Ghudran Formation (Parker, 1970): Jo

The Wadi Umm Ghudran Formation of central Jordan disconformably overlies the late Turonian the Ajlun Group (Wadi As Sir Limestone Formation). In central Jordan (Karak and Wadi Mujib sections), the Wadi Umm Ghudran Formation (Fig.2) has a threefold subdivision, in ascending order, the Mujib Chalk, Tafilah and Dhiban Chalk members (MacDonald 1965; Powell 1988, 1989 and Powell and Moh'd 2011, 2012): (Figs. 4, 6A and 6C). The formation has a reduced overall thickness in north Jordan (Wadi El-Ghafar and the Wadi Umm Ghudran type section) which was located basinward; here the threefold subdivision is less clearly represented. The formation in central Jordan is equivalent to the Menuha Formation of the Negev in Israel (Reiss et al., 1985; Meilijson et al 2014), the latter offset by ca. 100 km by the left-lateral Dead Sea Transform (Freund et al. 1970).

The *Mujib Chalk Member* is ca. 11 m thick and marks the lower member of the Wadi Umm Ghudran Formation, and is formed mainly of chalky limestone (Fig.4).

The *Tafilah Member* is ca. 65 m thick and is composed of marl, marly limestone with chert interbeds, the latter derived from silicoflagellates and radiolaria (Powell and Moh'd 2012); the macrofauna includes oysters and echinoids (Fig. 4). It is interpreted to be a shallow-water hemipelagic deposit (Powell 1988 1989).

The upper unit, the *Dhiban Chalk Member*, is ca. 18 to 30 m thick and is composed of chalky limestone rich in foraminifera. The base is marked by an oyster/coral encrusted hardground in Wadi Mujib, overlain by detrital phosphatic chalk passing up to chalk. (Powell and Moh'd 2012).

Alia Sandstone Formation: Jo

Although the tripartite Wadi Umm Ghudran Formation is well exposed adjacent to the Dead Sea rift valley margins, to the southeast (i.e. shorewards) in Jordan it passes laterally to the coeval Alia Sandstone Formation comprising (Fig.2) cross-bedded and *Thalassinoides*-burrowed siliciclastics, interbedded with marl, dolomite and thin chert beds (Powell 1989; Powell and Moh'd 2011).

Themed Formation (Ziko et al. 1993): Eg/S

The predominantly carbonate deposits of the Themed Formation are restricted to the north central area of the Sinai and are coeval with the mixed siliciclastic-carbonate deposits of the Matulla Formation in south Sinai and Eastern Desert (Ziko et al. 1993; Farouk and Faris 2012; Fig. 5). The Themed Formation unconformably overlies the Wata Formation of Turonian age; the upper part of the Wata Formation in this area is characterized by yellowish grey and brown, bioturbated, massive, stromatoporoidal limestone with some gastropods (*Nerinea* sp.) rich in worm tubes. The Themed Formation is overlain unconformably by the Sudr Chalk Formation of Campanian-Maastrichtian age (Fig.5). The thickness of the Themed Formation at the type locality is 160 m (Ziko et al. 1993), whereas in the Ras el-Gifa section it is reduced to 37 m. Here, the Themed Formation can be subdivided into two informal members:

Lower limestone Member is ca. 18 m thick and consists of argillaceous limestone intercalated with marl rich in oysters and echinoids.

Upper Chalky Limestone Member is ca. 19 m thick and consists of hemipelagic chalky facies. In view of the lack of distinctive vertical facies changes between the Themed and Sudr formations some authors (e.g., Khalil and Zahran 2014) considered the lower part of the Sudr Chalk Formation at Wadi El Mizeira (northeastern Sinai) to be Santonian in age. In the present study, the top of the Themed Formation is characterized by burrow-filled, argillaceous chalky limestone overlain by the Sudr Chalk, which is well-marked by a white, massive chalky limestone rich in planktonic foraminifera.

Matulla Formation (Ghorab 1961): Eg/S

The Coniacian-Santonian Matulla Formation ranges in thickness from 55 m at Gebel Nazazat to 65 m at Gebel Qabaliat. It is subdivided into three distinctive informal members (Fig. 5), namely i) the Lower Clastic Member, ii) the Middle Mixed Siliciclastic-Carbonate Member, and iii) the Upper Carbonate Member (Figs. 5 and 6B). The formation is equivalent, in part, to the Themed Formation of the southern Sinai and Eastern Desert (Fig. 2).

The Matulla Formation also unconformably overlies the Turonian Wata Formation and is overlain by the Sudr Chalk Formation (Figs. 2, 5 and 6B). A rich megafossil assemblage is recorded in middle member of the Matulla Formation, overlying a faunally barren interval. The most dominant macrofossils in the middle member include bivalves: *Pycnodonte costei* (Coquand), *Plicatula ferryi* Coquand, *Gyrostrea thevestensis* (Coquand), *Flemingostrea boucheroni* (Coquand). Issawi et al. (2009) in their stratigraphic study of the Matulla Formation in west Central Sinai, raised the rank of the formation to a group status embracing two formations; the Nubia Formation at the base (Taref Sandstone "Coniacian" and Quseir clastics "Santonian") and the Duwi Formation "Campanian" at the top, equivalent in the present study to Lower Clastic, Middle Mixed Siliciclastic-Carbonate, and Upper Carbonate members, respectively. According to Hermina (1990), the Taref Sandstone Formation (characterized mainly by cross-bedded sandstone, thinning towards the north) is considered Turonian in age, and the Quseir Variegated Shale of early Campanian age (Fig. 2). The Duwi Formation is distinguished by its economic phosphate beds southward in Egypt, but in Sinai only a few thin phosphatic limestones and coprolites are recorded (Ahmad et al. 2014). Therefore, in the present study, it is prefered to use the term Matulla Formation for these three informal members, although the upper part may be early Campanian in age and a correlative of the lower part of the Campanian Duwi Formation of southern Egypt. The unconformable boundary of the Matulla Formation with the underlying upper Turonian Wata Formation can be traced throughout the whole of the Sinai and Eastern Desert with a marked vertical lithofacies change from carbonates to siliciclastics. The presence of a 20 cm thick palaeosoil layer, including plant remains, at the base of the Duwi Formation (equivalent in the present study to the Upper Carbonate Member) indicates an unconformable relationship between the upper Campanian Duwi Formation and the underlying Santonian to lower Campanian Matulla Formation (Issawi et al. 2009). The upper boundary of the Matulla Formation with the overlying Sudr Chalk Formation is unconformable throughout the Sinai and Eastern Desert. This boundary is well marked in the field (Fig. 6B) where the Sudr Chalk Formation is characterized by its white chalky limestone, indicating a period of marine transgression, above the brownish colour of the regressive mixed siliciclastic-carbonate Matulla Formation (Lüning et al 1998; Samuel et al. 2009; Farouk and Faris 2012; Farouk, 2015). The disconformble boundary is also present in to the north in the Negev, Israel (Honigstein et al. 1987; Almogi-Labin et al. 1991 and 1993; Meilijson et al. 2014).

Sudr Chalk Formation

In Sinai the Sudr Chalk Formation is divided into: the Campanian Markha Member, composed of chalky limestone rich in *Pycnodonte vesicularis* (Lamarck) with chert and phosphate nodules, especially at the base, and the Maastrichtian Abu Zenima Member, composed of chalky limestone representing high rates of carbonate sedimentation in outer-ramp locations across most of northern Egypt (Farouk and Faris 2012; Farouk 2014). This definition of the Sudr Chalk Formation is applicable in the south where the chert is present, and towards the north, where chert is absent

Biostratigraphy

The biostratigraphic framework of the investigated successions is based mainly on planktonic foraminifera and calcareous nannofossils. The presence of many intervals barren of planktonic foraminifera and containing only sparse calcareous nannofossils, may be due to high energy, shallower-marine lithofacies in central Jordan (Tafilah Member and Alia Formation; Powell 1989), and in some intervals in the Matulla Formation (Egypt). Five nannofossil zones and three Tethyan planktonic foraminiferal zones were identified in the present study, based on the lowest and highest occurrence (LO, HO) of the marker species (Figs. 7-9). The most biostratigraphically significant planktonic foraminifera and calcareous nannofossils are illustrated in Figs. 10 and 11.

Calcareous nannofossils

The CC nannofossil zonation of Sissingh (1977) and Perch-Nielsen (1985) is used in the present study. The following five nannofossil biozones are recognised: *Lucianorhabdus malefomis* (CC12), *Micula staurophora* (CC14), *Reinhardtites anthophorus* (CC15), *Lucianorhabdus cayeuxii* (CC16), and *Broinsonia parca* (CC18) zones (Figs. 7 and 8). *Lucianorhabdus malefomis (CC12) Zone*: this is defined by the LO of *Luianorhabdus malefomis* Reinhardt to the LO of *Mathasterites furcatus* Deflandre. *L. malefomis* is very rare or absent in open-ocean settings, where *Eiffellithus eximus* (Stover) is a better marker taxa (Perch-Nielsen, 1985). Burnett (1998) noted that the LO of *E. eximus* occurs within Subzone UC8a, which can be correlated with the base CC12 Zone and, furthermore, can be used as zonal marker according to Gradstein et al.

(2012).The base of this zone was not determined in the studied sections which are stratigraphically higher. Representative taxa are recorded from the upper parts of the Turonian Wadi As Sir Limestone (Jo) and Wata (Eg/S) formations. The preservation, abundance and diversity of the calcareous nannofossils fluctuate markedly within the deposits of the CC12 Zone. The Karak and Wadi El-Ghafar (Jo) sections record a moderate preservation of calcareous nannofossils which are common to abundant with a relatively high diversity, whereas the Wadi Mujib section (Jo) and other sections in Egypt, yielded relatively sparse and poorly preserved calcareous nannofossils probably as a result of dolomitization and shallowing palaeoenvironments. However, the assemblages of the CC12 Zone are generally dominated by *Watznaueria barnesae* (Black), *W. biporta* Bukry, *Zeugrhabdotus erectus* (Deflandre in Deflandre & Fert), *Cyclagelosphaera margerelii* Noël, *Eprolithus floralis* Stradner, *Calcicalathina alta* Perch-Nielsen, *Eiffellithus eximus* (Stover), *Eiffellithus turriseiffelii* (Deflandre *in* Deflandre & Fert), *Praediscosphaera spinosa* (Bramlette & Martini), and *Radiolithus planus* Stover (Fig. 8). A late Turonian age is inferred for this zone.

Micula staurophora (CC14) Zone: This zone is defined by the LO of *Micula decussata* (Gardet) to the LO of *Reinhardtites anthophorus* (Deflandre). The *Micula staurophora* (CC14) Zone of middle–upper Coniacian is recorded from the Mujib Chalk Member in the Karak section (Jo) and the lower Themed Formation of the Ras el Gifa section (Eg/S). In Egypt it is found to be absent in the Matulla Formation as a result of the shallower, siliciclastic nature of the palaeoenvironment. The preservation of calcareous nannofossils of the CC14 Zone is generally poor. It overlies directly CC12 Zone of late Turonian age, which is recorded from the Wadi As Sir Limestone Formation in Jordan and the equivalent Wata Formation in Egypt. In general, the identified taxa in this zone are rare, with moderate diversity. The assemblage of this interval is similar to that of the underlying CC12 Zone, with the addition of occurrences of the nominate taxon (Fig. 8). A Coniacian age is indicated.

Reinhardtites anthophorus (CC15) Zone: It is defined by the LO of *Reinhardtites anthophorus* to the LO of *Lucianorhabdus cayeuxii* Deflandre. This zone is recorded in the Wadi El-Ghafar (Jo), and Ras el Gifa sections (Eg/S) (Fig. 9). In the Karak and Wadi Mujib sections (Jo), this biozone is missing, where the LO of *Lucianorhabdus cayeuxii* and *Reinhardtites anthophorus* appear together in sample 144 in the Karak section and sample 84 above the barren interval in the Wadi Mujib section or very shallow marine deposited including only some sporadic microplanktonic fauna. The dominant taxa are similar to those of the underlying CC14 with the addition of the *Broinsonia parca expansa* Wise & Watkins *in* Wise 1983 and *Reinhardtites anthophorus* (Fig. 8). The stratigraphic age of CC15 Zone was thought to coincide approximately with the earliest Santonian (e.g., Robaszynski et al. 1990; Hardenbol et al. 1998; Gradstein et al. 2012). However, the recently erected GSSP in northern Spain places this zone in the late Coniacian (Lamolda et al. 2014; Fig. 9) in accordance with the present study.

Lucianorhabdus cayeuxii (CC16) Zone: this is defined by the LO *Lucianorhabdus cayeuxii* to the LO of *Calculites obscurus* (Deflandre). Zone CC16 is present in all sections measured in Egypt and Jordan (Fig. 9). The upper part of this biozone could not be delineated owing to the absence of the marker species *Calculites obscurus* due to a major unconformity. An early Santonian age is indicated.

Broinsonia parca parca (CC18) Zone: this is defined by the LO of *Broinsonia parca* (Stradner) *parca* Bukry to the HO *Marthasterites furcatus* (Deflandre *in* Deflandre & Fert). It is recorded in all the studied sections (e.g. Upper Carbonate Memember of the Matulla Formation andbasal Sudr Chalk Formation in Egypt or the equivalent Dhiban Chalk Member and the overlying

Amman Silicified Limestone Formation in Jordan). As a result of the major early Campanian marine transgression calcareous nannofossils are common, with moderate to good preservation. The dominant species in this zone are: *Watznaueria barnesae* (Black in Black & Barnes), *Watznaueria bioporta* Bukry, *Eiffellithus eximius, Prediscosphaera cretacea* (Arkhangelsky), *Cribrosphaerella ehrenbergii*, *Retecapsa crenulata* (Bramlette & Martini), and *Tranolithus orionatus* (Reinhardt), as well as rare forms of *Broinsonia parca constricta* Hattner and Wind, *Arkhangelskiella cymbiformis* Vekshina and *Chiastozygus litterarius* (Górka) (Fig. 8). In the present study, the CC18 Zone overlies directly CC16 Zone; the *Calculites obscurus* (CC17) Zone, based on the interval from the LO of *Calculites obscurus* to the LO of *Broinsonia parca parca* is absent in all the studied sections due to the unconformity at the Santonian/Campanian boundary (Fig.9). However, Farouk and Faris (2012) recorded this zone in the Mitlla Pass section, Egypt, about 8 km from the Ras el Gifa section indicating the local irregularity of this unconformity.

Planktonic foraminifera

The planktonic foraminiferal data and a summary of their biostratigraphy are presented in Figs. 7-9. Preservation of the planktonic foraminifera varies from moderate to poor through the studied sections. The low-latitude Tethyan planktonic foraminiferal biozonations of Caron (1985) and Robaszynski et al. (2000) are used in the present study.

Dicarinella concavata Zone: This zone covers the interval from the LO of *Dicarinella concavata* (Brotzen) to the LO of *Dicarinella asymetrica* (Sigal). It is recorded from the lower part of Wadi Umm Ghudran Formation (Mujib Chalk Member in central Jordan), whereas in Egypt, the equivalent interval is nearly barren of planktonic foraminifera; it may be correlative with ammonite zones *Barroisiceras onilahyense* Basse, *Metatissotia fourneli* Bayle and *Subtissotia africana* (Perou) of Coniacian age (Obaidalla and Kassab 2002) (Figs. 4 - 5).

Poor to moderately preserved planktonic foraminifera are recorded in this zone, including *Whiteinella*/*Hedbergella* spp., *Dicarinella primitive* Dalbiez, *D. imbricate* (Mornod), *Contusotruncana fornicata* (Plummer) and *Heterohelix globulosa* (Ehrenberg) in addition to the zonal marker (Fig. 9). This zone is equivalent to upper part of CC12 to CC14 nannofossil zones of late Turonian - Coniacian age as mentioned in many standard schemes (e.g., Premoli Silva and Sliter 1999; Gradstein et al. 2012; Haq 2014; Coccioni and Premoli Silva 2015). In the present study, the LO of the zonal marker is recorded above the Turonian/Coniacian unconformity which is also marked by the absence of CC13 nannofossil zone. In low-latitude successions such as in Tunisia, Egypt and the present study the LO of *D. concavata* is stratigraphically relatively high with the index-species first appearing in the late Coniacian CC14 nannofossil Zone (e.g. Caron 1985; Nederbragt 1991; Abdel-Kireem et al. 1995; Farouk and Faris 2012; Elamri et al. 2014). The zone spans the Coniacian Stage.

Dicarinella asymetrica Zone: This zone is defined as the Total Range of *Dicarinella asymetrica*. It is recorded in the upper part of the Tafilah Member of the Wadi Umm Ghudran Formation and upper chalky limestone in the Themed Formation at the Ras el-Gifa section. Al-Rifaiy et al. (1993) observed the absence of the marker zonal boundary taxon *Dicarinella asymetrica*, and assigned a late Coniacian age for the whole of the Wadi Umm Ghudran Formation in Jordan. However, the zonal marker is consistently present, but never abundant, and uncommon in the shallow-water lithofacies (e.g. Wadi Mujib section). The occurrence of *Dicarinella asymetrica* in the studied sections corresponds to CC16 nannofossil Zone (Fig. 9). The *Dicarinella asymetrica* Zone occurs in the Santonian Stage as noted in many of the standard schemes across different palaeolatitudes (e.g. Caron 1985; Premoli-Silva and Sliter 1999; Gradstein et al. 2012; Haq 2014; Meilijson et al. 2014). The preserved (lower) part of the *Dicarinella asymetrica* Zone as indicated by the equivalent CC16 nannofossil zone includes well-preserved and abundant *Dicarinella asymetrica, Marginotruncana sinusoa* Porthault and *M. undulata* (Lehmann). In the present study, most of the upper Santonian *Dicarinella asymetrica* Zone is missing due to the depositional hiatus that spans the equivalent CC17 Zone. The zone spans the Santonian Stage, although the upper part is not represented in the studied sections due to a depositional hiatus.

Globotruncanita elevata Zone: This zone was defined as the partial range zone from the HO of *Dicarinella asymetrica* to the LO of *Globotruncana ventricosa* White. Planktonic foraminifera are abundant, with moderate to good preservation. This interval is characterized by the HOs of *Marginotruncana* and *Dicarinella*, and the abundance of several species of *Globotruncana*. It is also characterized by the LOs of *Globotruncana arca* (Cushman), and *G. bulloides* Vogler. This zone spans the equivalent calcareous nannofossil zones CC17-CC18 and CC19 indicating an early Campanian age (Gradstein et al. 2012).

Stage boundaries

Many stratigraphical problems have been observed relating to the correlation of Coniacian – Campanian biostratigraphic events across different palaeolatitudes in recent years (Farouk and Faris 2012; Razmjooei et al. 2014; Coccioni and Premoli Silva 2015). This has led to the establishment of several different planktonic foraminiferal and calcareous nannofossil zonal schemes with different age assignments, as noted above. To resolve this issue, it may be necessary to study the boundaries in a much broader context based upon integrated biostratigraphy. The palaeogeographic applicability of biostatigraphic zonations is influenced by palaeolatitudinally controlled temperature gradients and the niche preferences of marker species (Bralower et al. 1995).

The Turonian/Coniacian (T/C) boundary

At the proposed GSSP (Walaszczyk et al. 2010) in Salzgitter-Salder Quarry (Lower Saxony, Germany) and the Słupia Nadbrzeżna river-cliff section (central Poland), the T/C boundary falls within the *Dicarinella concavata* Zone and nannofossil Zone CC13, between the first occurrence of *Broinsonia parca parca* and the last occurrence of *Helicolithus turonicus* Varol & Girgis. However, the T/C boundary in the present study area is represented by the unconformity surface (e.g. base of the Mujib Chalk Member) and the absence of both the nannofossil Zone CC13 and the equivalent lower part of *Dicarinella concavata* Zone. Walaszczyk et al. (2010) reported that the *Broinsonia parca parca* Zone falls into the lower Coniacian. In the present study and previous publications covering the southern Tethys, the LO of the marker zone *Broinsonia parca parca* appears stratigraphically higher, up to the lower Campanian (Perch-Nilsen 1985; Burnett 1998; Gradstein et al. 2012; Farouk and Faris 2012). This may be the result of provincialism at different palaeolatitudes. In the present study, the precise biostratigraphical determination of the T/C boundary is hampered by the unconformity surface and depositional hiatus marked by the absence of nannofossil Zone CC13.

The Coniacian/Santonian boundary

According to the GSSP definition, the base of the Santonian falls in the lower part of the *Dicarinella asymetrica* Zone and nannofossil Zone CC16 (Lamolda et al. 2014). At the GSSP in northern Spain and the Gubbio section in Italy the *D. asymetrica* Zone is taken lower down in the upper Coniacian (Lamolda et al. 2014; Coccioni and Premoli Silva 2015). However, Lamolda et al. (2014) used the first common occurrence of *D. asymetrica* to define broadly the base Santonian in the palaeotropics. In other Neo-Tethyan provinces, especially in the Middle East, the LO of *D. asymetrica* is also used to define the base of the Santonian Stage (e.g., Caron 1985; Premoli Silva and Sliter 1995; Robaszynski et al. 2000; Petrizzo 2000, 2002; Sari 2006; Farouk and Faris 2012; Gradstein et al. 2012) although Meilijson et al. (2014) take the boundary slightly higher. These variations in the stratigraphic range of planktonic foraminifera are also observed in the nannofossil zonation, where the most important marker species (e.g., *Lithastrinus grillii* Stradner and *Lithastrinus septenarius* Forchheimer) were not recorded in the present study as a result of provincialism in the faunas across Neo-Tethys.

The Santonian/Campanian boundary

The Santonian/Campanian boundary is, according to Perch-Nielsen (1985), taken to lie somewhere within nannofossil Zone CC17, and the upper part of UC12 Zone according to Burnett (1998), below the FO of *A. cymbiformis*, and *B. parca constricta*. The same observation is found in the time-scale chart of Gradstein et al. (2012) and Haq (2014). Gale et al. (2008) proposed the Santonian/Campanian boundary stratotype section (i.e. the Waxahaxhie Dam Spillway section of north Texas, USA), and noted that the last appearance of *Dicarinella asymetrica* coincided with the first appearance of the calcareous nannofossil subspecies *Broinsonia parca parca* and *Broinsonia parca constricta* that corresponds approximately to the Austin/Taylor unconformity.

Many authors noted that *Broinsonia parca parca* appears higher in the lower Campanian above *Arkhangelskiella cymbiformis* (Perch-Nielsen 1985; Burnett 1998; Gradstein et al. 2012). The LO of *Arkhangelskiella cymbiformis* should be referred to lower Campanian UC13 Zone

(Burnett, 1998). Other authors note that the *Arkhangelskiella cymbiformis* and *B. parca parca* may lie somewhere within the upper Santonian Stage, coincident with the interval recorded below the Santonian-Campanian Boundary Event (SCBE), such as at Gubbio (Voigt et al. 2012) and in Iran (Razmjooei et al. 2014). Gale et al (2008) recorded the joint LO of *B. parca parca* and *B. parca constricta* (= base of nannofossil Subzone UC14b) above the Austin/Taylor unconformity. Farouk and Faris (2012) noted that rare specimens of *A. cymbiformis* have been observed in the late Santonian (CC17) and, furthermore, Gale et al. (2008) recorded the LO of *A. cymbiformis* near the base of nannofossil Subzone UC13a, indicating that the range of the *A. cymbiformis* extends down into the Santonian. In the present study, the LO of *A. cymbiformis* is recorded at Wadi El-Ghafar section within the equivalent planktonic foraminifera *D. asymetrica* Zone indicating a late Santonian age.

Many authors have noted the extended HO of *Marginotruncana* spp. into the basal Campanian stage (e.g., Farouk and Faris 2012; Elamri et al. 2014), while the HO of *Dicarinella asymetrica* has been interpreted in two different approaches in planktonic foraminifera biostratigraphy: the first considers the HO of *Dicarinella asymetrica* to correspond to Santonian/Campanian boundary (Caron 1985; Robaszynski et al. 2000; Sari 2006; Gradstein et al. 2012; Elamri et al. 2014; Haq 2014; Meilijson et al. 2014; Coccioni and Premoli Silva, 2015); the second considers that it extends to earliest Campanian age (e.g., Premoli Silva and Sliter 1995; Petrizzo 2000, 2002; Gale et al. 2008; Ardestani et al. 2012). The marker species of calcareous nannofossil CC18 Zone, *B. parca parca*, appears together in most studied sections above the Santonian/Campanian unconformity surface which is associated with the sharp extinction of *Dicarinella* and *Marginotruncana*, and the presence of relatively abundant *Globotruncanita* and *Globotruncana* genera that characterize the *Globotruncanita elevata* Zone.

Microplanktonic zonation: discussion

Jordan

In Jordan, no detailed microplanktonic biostratigraphy has been carried out to date based on an integrated study of calcareous nannofossils and planktonic foraminifera. Such integrated studies are considered to provide a higher resolution biostratigraphy than the use of either group alone. Little research has been conducted on the microplanktonic biostratigraphy of the Coniacian–Campanian Wadi Umm Ghudran Formation in Jordan, a period of significant change in sea level, bioproductivity and sedimentation on the Arabian Platform following marine drowning of the Turonian rimmed carbonate platform (Flexer et al. 1986; Reiss et al 1985; Almogi-Labin et al 1993; Powell and Moh'd 2011; Meilijson et al. 2014). Three different age-determinations have been proposed for this formation in Jordan: 1) late Coniacian (for the whole formation) (Al-Rifaiy et al. 1993); 2) Coniacian-Santonian (Koch 1968; Mustafa 2000; Mustafa et al. 2002) and 3) a Coniacian-Campanian age (e.g., Powell 1988, 1989; Moh'd 2000; Powell and Moh'd 2011). The Wadi Umm Ghudran Formation is here assigned to a Coniacian–Campanian age based on the identified calcareous nannofossil assemblages. The latter range from *Micula staurophora* (CC14), *Reinhardtits anthophorous* (CC15) and *Lucianorhabdus cayeuxii* (CC16), to *Broinsonia parca parca* (CC18). The equivalent planktonic foraminifera zones are *D. concavata*, *D. asymetrica* and *G. elevata*. Absence of the lower Coniacian CC13 Zone and the upper Santonian *Calculites obscurus* (CC17) Zone indicates three periods of depositional hiatus, namely, at the Turonian-Coniacian boundary (Wadi As Sir Limestone Formation – Mujib Chalk Member boundary), the Coniacian-Santonian boundary (within Tafilah Member) and the Santonian-Campanian stage boundary (base of the Dhiban Chalk Member). These disconformities are represented by bioerosive hardgrounds at the top of the Wadi As Sir Limestone Formation and at the top of the Tafilah Member (Powell and Moh'd 2012).

Egypt (Sinai)

The Matulla Formation is characterized by relatively sparse and poorly preserved microplanktonic assemblages due to the nature of the nearshore, shallower-water palaeoenvironments. Many authors consider the Matulla Formation to be Coniacian-Santonian in age and that the Sudr Chalk Formation marks the base of the Campanian (e.g., Shahin and Kora 1991; Farouk 2015). Other authors assigned a lower Campanian age to the Upper Carbonate Member of the Matulla Formation (Abdel-Gawad et al. 2004) or with equivalent Duwi Formation of the Matulla Group (Cherif et al. 1989; Issawi et al. 2009; Attia et al., 2013). In the present study, the Upper Carbonate Member of the Matulla Formation contains sparse and low diversity calcareous nannofossils. The assemblage recorded at Gebel Qabaliat, includes *Watznaueria barnesae*, *W. biporta*, *Quadrum gartneri*, and *Quadrum sissinghii.* Furthermore, this member is overlain by the Sudr Chalk Formation yielding *Globotruncanita elevata* Zone of early–middle Campanian age. The presence of *Quadrum sissinghii* in the Upper Carbonate Member may reflect an earliest Campanian age for the uppermost part of the Matulla Formation. In addition to the LO of *G. elevata* in the southern Tethys, this species was found considerably later, just above the Santonian/Campanian boundary (e.g., Farouk and Faris 2012; Meilijson et al. 2014).

The Upper Carbonate Member correlates well with the Phosphate-bearing Unit of the Matulla Formation, which is recorded from the Esh El Mallaha area, Egypt (Cherif and Ismail 1991; Ismail 2012). These authors noted that this Unit might be of Campanian age as it is overlain by chalk yielding late Campanian age *Globotruncanita calcarata* Zone.

Lithofacies associations

Twenty-six lithofacies types (FT) have been identified and are briefly described in Table 1 and illustrated in Figs. 12 to 13. These facies types are grouped into six lithofacies associations that have been assigned to six depositional environments, the latter ranging from: a littoral siliciclastic facies belt, peritidal carbonate facies belt, intertidal carbonateramp deposits**,** high-energy ooid shoals and shelly biostromes, shallow subtidal facies belt, and pelagic facies belt. These lithofacies associations are described below in relation to their depositional environments. The distribution of the different lithofacies recognized throughout the Wadi Ghudran Formation (Jo) and the Matulla Formation (Eg/S) is illustrated in Figs. 4 and 5.

Littoral siliciclastic facies belt

This facies belt is recorded from the Lower Clastic Member of the Matulla Formation (Eg/S) (and its equivalent, the Alia Sandstone Formation in southeast Jordan; Powell 1989). It comprises four facies types: glauconitic ferruginous siltstone and shale (FT1), calcareous glauconitic quartz arenite (FT2), quartz arenite (FT3); the last facies and sandy evaporitic recrystallized lime-mudstone (FT4) are recorded from the upper part of the Middle Mixed siliciclastic-carbonate Member of the Matulla Formation. The Alia Sandstone mostly comprises FT2 and FT3 (Powell 1989). The scarcity of fauna and bioturbation suggests deposition under restricted shallow-marine conditions in a wide intertidal to peritidal-flat siliciclastic setting, with pulses of terrigenous siliciclastics derived from the hinterland located to the south and southeast. The high maturity of the quartz arenite indicates deposition in high-energy, shallow-water in a lower shoreface environment (Pettijhon et al. 1987; El-Azabi and El-Araby 2007; Wanas 2008).

High maturity quartz suggests derivation from mature Lower Palaeozoic and/or Lower Cretaceous sandstones of the Arabian Craton (Powell et al. 2014).

Peritidal carbonate facies belt

This lithofacies belt consists mainly of dolomitic mudstone with two facies types: sandy ferruginous sandy dolomicrite (FT5) and ferruginous glauconitic dolomicrite (FT6). It is recorded in the upper part of both Lower Clastic and Middle Mixed siliciclastic-carbonate members of the Matulla Formation (Eg/S) (Fig. 5) and the upper part of the Tafilah Member (Jo). The size and fabric of the dolomite rhombs, lime-mud relicts and sand content suggest it was formed from early diagenetic dolomitization of an original sandy lime-mudstone in a peritidal setting (Powell and Moh'd 2012). The quartz sand is either fluvial in origin or derived from offshore-onshore storm events. The finely crystalline dolomite with rare evaporites is interpreted as being deposited in the upper intertidal to supratidal zone of inner platform during a sea-level fall (Wanas 2008).

Intertidal carbonate ramp deposits

This lithofacies belt is represented mainly by the Upper Carbonate Member of the Matulla Formation (Eg/S) and the Tafilah Member (Jo) of the Wadi Umm Ghudran Formation (Figs. 4 and 5). Facies types comprise: coarse-grained dolomitic mudstone (FT7), siliceous recrystallized lime-mustone (FT8), recrystallized dolomicrite (FT9), glauconitic sandy phosphatic lime-mudstone (FT10), ooidal bioclastic wacke/packstone (FT11) and chert-bearing facies (FT12) together with sparse calcareous claystone. Sparse, low-diversity bivalves are present in the lower part of this facies association, including: *Pycnodonte vesicularis hippodium* and *Py. vesicularis nikitini*. The bivalve fauna and lithofacies suggest deposition in a shallow subtidal environment below normal wave base. Towards the top, the scarce, low-diversity fossils preserved in a lime–mud matrix with floating quartz sand grains suggest deposition in a restricted lower intertidal regime (Wilson 1975; Flügel 2004).

High-energy ooid shoals and shelly biostromes

This lithofacies association is recorded in the Themed (Eg/S) and Wadi Umm Ghudran (Jo) formations, represented by onco-ooid packstone (FT13) and glauconitic peloidal packstone (FT14), indicating a moderate to high-energy, intertidal shoal depositional environment (Kostic and Aigner 2004).

Shallow subtidal facies belt

This lithofacies association (FT15 to FT 23) is predominantly recorded in the Matulla Formation and lower unit of the Themed Formation (Eg/S) in addition to the Tafilah Member (Wadi Umm Ghudran Formation (Jo)). In the Matulla Formation, this facies association is represented by shallow subtidal, mixed siliciclastic-carbonate shelf lithofacies including molluscan wacke/ packstone intercalated with calcareous claystone. The composition and texture suggest deposition in a shallow subtidal environment (Flügel, 2004).

In the Themed Formation, this facies association consists of argillaceous limestone intercalated with fossiliferous marl containing oysters and echinoid fragments. The microfacies are represented mainly by bioclastic wacke/packstone (FT17 and FT18), sandy bioclastic packstone (FT20) and oncoidal bioclastic packstone (FT21). The lack of open-marine biota such as ammonoids and planktonic foraminifera, contrasting with abundant echinoids and oysters, as well as the predominance of argillaceous limestone, reflects a fully marine, lagoonal environment. In the Wadi Umm Ghudran Formation (Jo), this facies consists of bioclastic wacke/packstone (FT17 and FT18), bio-intraclastic sandy packstone (FT24) and lime-mudstone (FT16) (Fig. 4).

Pelagic facies

This lithofacies consists of hemipelagic chalky facies and includes two facies types (Table 1): foraminiferal lime-mud (FT25) and foraminiferal wacke/packstone (FT26). It is recorded from the upper unit of the Themed Formation, Sudr Chalk Formation (Eg/S), and from the Mujib Chalk (lower part) and the Dhiban Chalk members of the Wadi Umm Ghudran Formation (Jo). This facies association is characterized by abundant and high-diversity, well-preserved planktonic and benthic foraminifera embedded in a dense lime mud interpreted as a pelagic facies of deep subtidal to middle shelf environments.

Depositional model

Regional variations in sedimentary facies from carbonate ramp facies towards the north, to mixed siliciclastic/carbonate facies in the south and southeast, are attributed to their relative palaeogeographic positions on a homoclinal ramp at the southern margin of the Neo-Tethys Ocean (Powell and Moh'd 2011). The variations in the relative palaeogeographic position and water depth were influenced to a large extent by compressive deformation and variable regional uplift of the former stable platform of northeast Africa and Arabia as a result of deformation of the Syrian arc fold belt (Krenkel 1924; Shahar 1994).

In general, during Coniacian-Santonian time, a carbonate facies belt was prevalent in the northward areas of the outer ramp (including the Themed Formation in North Sinai and

Wadi Umm Ghudran Formation in central/north Jordan). The three members of the Wadi Ghudran Formation are interpreted as having formed under fluctuating deeper and shallower-marine settings on a pelagic ramp (Powell and Moh'd 2011). The lateral passage to a mixed siliciclastic/carbonate facies belt of the Matulla Formation (Eg/S) and Alia Formation (Jo) was probably in response to hinterland uplift and siliciclastic progradation in south Egypt and the Arabian Craton. The increase in siliciclastics to the southeast is consistent with regional trends seen in Egypt (Bauer et al. 2002; El-Azabi and El-Araby 2007; Farouk and Faris 2012).

In southern Egypt the Coniacian to Santonian succession is missing (Hermina 1990) or is represented by alluvial lithofacies (Nubia Sandstone) (Figs. 2, 14). Farther east, in Saudi Arabia, the Coniacian to Santonian succession is also missing. Here, the Cenomanian-Turonian Wasia Formation is disconformably overlain by the Campanian-Maastrichtian Aruma Formation (Powers et al. 1966). In the subsurface of the North Western Desert of Egypt, shallow-water carbonate deposits are observed in the Abu Roush Formation (Issawi et al. 2009).

The Matulla Formation (Eg/S) was deposited predominantly in shallow-marine environments, and exhibits rapid vertical lithofacies changes with twenty-four siliciclastic and carbonate lithofacies. The lithofacies associations are assigned to three main depositional environments: a) marginal-marine inner ramp (including siliciclastic shelf, peritidal carbonate facies shelf, and mixed siliciclastic-carbonate shelf), b) intertidal carbonate platform deposits, and c) high-energy ooid shoals and shelly biostromes). Towards the north, increased carbonate productivity is observed in the coeval Themed Formation indicating deposition in a shallow-marine environment with oscillations from intertidal to deep subtidal (Fig. 14). In contrast, the depositional environment of the chalk lithofacies in north and central Jordan represents a pelagic carbonate ramp, with co-eval off-shore sand banks forming the sandy facies in southeast Jordan

(Alia Formation of Powell and Moh'd 2011; Makhlouf et al. 2015). During the Coniacian, the peritidal flat facies association present in southwestern Sinai changed, in response to rising sea-level, to a carbonate ramp towards North Sinai and Jordan. This predominant carbonate lithofacies belt includes the Themed Formation in north Sinai, Wadi Umm Ghudran Formation in Jordan and Abu Roush Formation in subsurface of the Western Desert). In north Sinai a shallow subtidal lagoonal environment is characterized by an abundant macrofauna. These varied lithofacies become less prominent towards the north in Jordan (Wadi El-Ghafar) and Negev/Galilee, Israel (Reiss et al. 1985; Meilijson et al. 2014), where the shallow-water siliciclastic lithofacies are absent, being replaced by deeper water chalks and marls with abundant microplanktonic faunal assemblages. Mixed carbonate-chert-phosphorite sedimentation was quickly established over a wide area during the late Campanian following a rapid relative sea-level rise in the early Campanian (Pufahl et al. 2003; Abed et al. 2007; Powell and Moh'd 2011).

Sequence stratigraphic interpretation

The sequence stratigraphic interpretation of the Coniacian-Campanian succession in north-eastern Egypt and Jordan is based on the observed microplanktonic biostratigraphy and lithofacies associations, as well as the nature of the sequence boundaries that separate the latter. This analysis allows a better understanding of the evolution of base-level changes during Coniacian-Santonian time, and also helps to explain the significant lateral changes of lithofacies, their biostratigraphical correlation and temporal relationships. The distribution of lithofacies belts and their microfauna indicates the interplay between tectonic uplift (intra-plate Syrian Arc deformation) and eustatic sea-level fluctuations. Four major sequence boundaries have been recognised, coincident with the Turonian/Coniacian (Tu/Co1), Coniacian/Santonian (Co/Sa2) and Santonian/Campanian (Sa/Ca3) stage boundaries, and intra-early Campanian (Ca/4). The presence of these boundaries is also recognized biostratigraphically across the study area (Figs. 10 and 15). These correlatable surfaces define three 3rd-order depositional sequences, each consisting of transgressive (TST) and highstand systems tracts (HST). HSTs are usually thicker than TSTs due to increased accommodation space during the HST. These TST–HST sequences are named according to their area of definition (e.g. depositional sequence Egypt and Jordan, DS Eg/Jo1–3) and are described briefly below (Figs. 15 and 16). Similarly, sequence boundaries (SB) are named according to their assigned stage boundaries, e.g. SB Tu/Co1, SB Co/Sa2, SB Sa/Ca3, and SB Ca4).

Sequence boundary 1: SB Tu/Co1

A rapid fall in relative sea-level in late Turonian to early Coniacian time resulted in a depositional hiatus during the early Coniacian, including local karstification on the carbonate platform (West Bank, Israel-Palestine: Weiler and Sass 1972; Flexer et al. 1986). The Turonian/Coniacian unconformity is always characterized by a sharp and well-marked change in lithology, which can be easily recognized in the field (Fig. 6a), separating the upper Turonian carbonate platform termed the Wata Formation (Eg/S) and the equivalent Wadi As Sir Limestone Formation (Jo) from the overlying siliciclastics of the Matulla Formation (Eg/S) or the shallow hemipelagic carbonate facies of Themed (Eg/S) or Wadi Umm Ghudran formations (Jo). This sequence boundary in Jordan is characterized locally by highly fragmented limestone with an erosion surface that marks a major change in sedimentation from the rimmed platform carbonates of the Ajlun Group, below, to the predominantly hemipelagic ramp deposits above. The basal part of the Mujib Chalk Member locally contains abundant detrital clasts (phosphate; fish and marine reptile teeth and bone fragments), representing a condensed transgressive sequence, following a depositional hiatus, as the rimmed carbonate shelf (Ajlun Group) was flooded during a rapid sea-level rise during the Coniacian (Powell 1989; Powell and Moh'd 2011).

In addition to the regional vertical lithofacies changes, this sequence boundary is supported by an absence of calcareous nannofossil Zone CC13 in the studied sections, this zone marking the Turonian/Coniacian boundary according to the schemes of Sissingh (1977) and Perch-Nielsen (1985). This unconformity surface has been widely recorded previously from the surrounding areas such as the Negev, West Bank (Israel- Palestine), Egypt, Jordan and Iran (e.g., Weiler and Sass 1972; Reiss et al. 1985; Flexer et al. 1986; El-Azabi and El-Araby 2007; Powell and Moh'd 2011, 2012; Farouk and Faris 2012; Razmjooei et al. 2014; Fig. 16). A comparison with the revised eustatic charts of Haq (2014) generally shows a major fall in eustatic sea level termed KTu5 that characterizes the end of the Turonian (Fig. 16). This sequence boundary (SB) is correlated with SB4 of Powell and Moh'd (2011); K150 of Sharland et al. (2004), SB1 of El-Azaby and El-Araby (2007) and SB Co-5 of Farouk (2015).

Sequence boundary 2: SB Co/Sa2

This sequence is characterized by vertical facies changes between the Lower Clastic Member and Middle Mixed Siliciclastic-Carbonate Member of the Matulla Formation or the boundary between Unit 1 and Unit 2 of the Themed Formation in Egypt. In Jordan, it occurs within the Tafilah Member and coincides with vertical facies changes and absence of calcareous nannofossil CC15 Zone at Karak and Wadi Mujib (Jo). Current work indicates that this boundary is coincident with the Coniacian/Santonian boundary (Fig. 6C), although earlier work suggested that this boundary representsthe higher Santonian/Campanian boundary (Reiss et al. 1985; Powell 1989; Powell and Moh'd 2011, 2012). The regional vertical facies changes are associated with an erosional unconformity and depositional hiatus of different magnitudes at various localities (Figs. 2, 8, 9 and 16). SB Co/Sa2 is recorded in different parts of Egypt (Farouk and Faris 2012) and also corresponds to the revised eustatic sea-level curve KSa1 of Haq (2014). This sequence boundary is correlated with SB2 or SB3 of El-Azabi and El-Araby (2007) although a Coniacian-Santonian boundary age (their SB3) is preferred here for this surface rather than an intra-Coniacian age as indicated by the latter authors (Fig. 15).

Sequence boundary 3: SB Sa/Ca3

This sequence boundary is characterized by another erosional unconformity at the Santonian/Campanian boundary. The associated erosional unconformity coincides with the absence of *Calculites obscurus* (CC17) Zone and the equivalent major part of *D. asymetrica* planktonic foraminiferal Zone. In Jordan, it occurs at a limestone base of the Dhiban Chalk Member of the Wadi Umm Ghudran Formation between the CC16/CC18 calcareous nannofossil zonal boundary (Figs. 6c and 9). In Egypt, this sequence boundary represents the boundary between the Middle Mixed Siliciclastic-Carbonate Member and Upper Carbonate Member of the Matulla Formation. In the Ras el-Gifa section, uplift may have been greatest where the SB Sa/Ca3 and SB Ca4 are amalgamated, based on the absence of the lower part of the *G. elevata* Zone (Figs. 10, 15 and 16). This sequence boundary is correlated with Santonian/Campanian unconformity in the southern Tethys (e.g., Reiss et al. 1985; Powell 1989; Powell and Moh'd 2011, 2012; Farouk and Faris 2012; Ahmed et al. 2014; Meilijson et al. 2014; Farouk 2015). The base of the so-called 2nd Chalk Member and sequence boundary in the Negev (Israel) is also taken at the Santonian/Campanian boundary (base *G.elevata* Zone) (Meilijson et al. 2014) approximately coincident with the K160 Arabian Platform boundary of Sharland et al. (2004).

Sequence boundary 4: SB Ca4

This sequence boundary occurs within the *Globotruncanita elevata* Zone, and is easily recognized by its sharp, undulating erosion surface. It separates the Wadi Umm Ghudran Formation from the overlying Amman Silicified Limestone Formation in Jordan, whereas in Egypt it marks the boundary between the Matulla Formation (and the equivalent Themed Formation) from the overlying Sudr Chalk Formation. The Amman Silicified Limestone Formation is characterized by penecontemporaneous diagenetic chert folds (Fig. 6A), possibly resulting from deposition of unstable shallow-water silica (chert) sol (Steinitz 1981; Mikbel and Zacher 1986; Powell and Moh'd 2011).

A comparison with the revised eustatic charts of Haq (2014) shows a major fall in eustatic sea level towards the top of the *G.elevata* Zone (mid Campanian) (Fig. 15). The SB Ca4 boundary is marked by a regional hiatus in Egypt, Jordan, the Negev (Israel) and South Africa (El-Azabi and El-Araby 2007; Ovechkina et al. 2009; Powell and Moh'd 2011 and 2012; Farouk and Faris 2012; Meilijson et al. 2014; Farouk 2015). This supports the proposal of Farouk and Faris (2112) that the SB Ca4 sequence boundary is synchronous with the Austin/Taylor unconformity in north Texas (Gale et al. 2008), although the latter authors proposed that this unconformity marks the earlier Santonian/Campanian boundary. It also correlates well with a major fall in eustatic sea level (KCa3 at the 80 Ma) sequence boundary of the revised eustatic chart of Haq (2014) (Fig. 15).

Depositional sequences

Depositional sequence Eg /Jo1

Depositional sequence Eg/Jo1 is of Coniacian age and comprises the Lower Clastic Member of the Matulla Formation and Unit 1 of the Themed Formation in Egypt, whereas in Jordan it constitutes the Mujib Chalk and Tafilah members of the Coniacian Wadi Umm Ghudran Formation (Fig. 16). The sequence falls within the lower part of the planktonic foraminiferal *Dicarinella concavata* Zone and the *Micula staurophora* (CC14) and *Reinhardtites anthophorus* (CC15) calcareous nannofossil zones. This sequence is bounded at its base by SB Tu/Co1 and at the top by SB Co/Sa2 (Fig. 16).

TST: The Transgressive systems tract **(**TST) consists of pelagic facies of the Mujib Chalk Member in Jordan. In Egypt, it consists of shaley bioclastic packstone in the lower part of Unit 1 of the Themed Formation or thick-bedded glauconitic ferruginous siltstone, shale and calcareous glauconitic quartz arenite deposited in a pertidal to intertidal environment in the Lower Clastic Member of the Matulla Formation (Fig. 16). In the Matulla Formation, the HST consists of a widely-distributed marker dolostone recorded in Sinai and the Eastern Desert (El-Azabi and El-Araby 2007; Farouk 2015). In Jordan, it is characterized by carbonate-rich strata (lime-mudstone to bioclastic packstone) capped by high-energy intertidal shoals in both the Themed Formation and Tafilah Member of the Wadi Umm Ghudran Formation (Fig. 16).The maximum flooding surface (MFS) separates the TST and HST in all the studied sections.

Depositional sequence Eg/Jo2

Depositional sequence Eg/Jo2 is of Santonian age and comprises the Middle Mixed Siliciclastic-Carbonate Member of the Matulla Formation and Unit 2 of the Themed Formation in Egypt, whereas in Jordan it constitutes the upper part of Tafilah Member of the Wadi Umm Ghudran Formation (Figs. 6C and 16). The sequence falls within the upper part of *Dicarinella asymetrica* planktonic foraminiferal Zone and the *Lucianorhabdus cayeuxii* (CC16) calcareous nannnoplankton zones. This sequence is bounded at its base by SB Co/Sa2 and at top by SB Sa/Ca3 (Fig. 16).

TST: The TST consists of another cycle of pelagic chalky facies of the upper Tafilah Member in Jordan. In Egypt, it consists of Unit 2 of the Themed Formation and coeval shallow-marine Mixed Siliciclastic-Carbonate Member of the Matulla Formation (Fig. 16). The HST is recorded only in the Matulla Formation representing typical regressive facies (FT4 and FT6), separated by the MFS. In other successions the HST is absent, perhaps a result of a depositional hiatus.

Depositional sequence Eg/Jo3

Depositional sequence Eg/Jo3 is of early Campanian age and comprises the Upper Carbonate Member of the Matulla Formation in Egypt, whereas in Jordan it constitutes the the Dhiban Chalk Member of the Wadi Umm Ghudran Formation (Figs. 9C and 16). In the Themed Formation, this sequence (DS Eg/Jo3) is absent, where the sequence boundaries Sa/Ca-3 and Ca-4 are amalgamated (Fig. 16). The sequence falls within the lower part of *Globotruncanita elevata* planktonic foraminiferal Zone (as defined in this paper) and the lower part of the *Broinsonia parca parca* (CC18) Zone. This sequence is bounded at base by SB Sa/Ca3 and at top by SB Ca4 (Fig. 16).

TST: The TST consists of pelagic facies of the Dhiban Chalk Member in Jordan. In Egypt, it may be coeval with Upper Carbonate Member of the Matulla Formation. The HST is recorded only in the Matulla Formation and is separated by a MFS, represented by an upward change from shallow subtidal to peritidal lithofacies, the latter consisting of typical regressive lithofacies facies (FT4 and FT6). In the Dhiban Chalk Member the HST is absent and the MFS is not recognized, whereas in the Matulla Formation it consists of FT9 and FT10. The top of sequence Eg/Jo3 is characterized by the prominent SB Ca4 near the base of a new major transgressive phase represented by the Sudr Chalk (Eg/S) or the equivalent Amman Silicified Limestone Formation (Jo).

Conclusions

Four broadly coeval rock units of Coniacian to Campanian age are recognized in the present study, termed from north to south: Wadi Umm Ghudran Formation (hemipelagic chalk-chert-phosphorite) and Alia Sandstone Formation in Jordan, Themed Formation in north Sinai (predominantly carbonate deposits) which passes laterally to the Matulla Formation (mixed siliciclastic-carbonate shelf). The Wadi Umm Ghudran Formation is assigned a Coniacian–Campanian age based on the identified calcareous nannoplankton assemblages: *Micula staurophora* (CC14), *Reinhardtites anthophorus* (CC15), *Lucianorhabdus cayeuxii* (CC16) and *Broinsonia parca parca* (CC18). Their equivalent planktonic foraminifera zones range from *Dicarinella concavata*, to the lower part of *D. asymetrica* and *Globotruncanita elevata.* The recorded calcareous nannoplankton biozones in the Themed Formation range from CC14 to CC16 indicating a Coniacian to Santonian age, whereas the siliciclastic Matulla Formation is nearly barren. Discrepancies in the observed stratigraphic ranges of a number of different key marker taxa that have been reported from different palaeolatitudes (e.g. Italy, America, Europe and southern Tethyan sites) are confirmed in present study. These discrepancies might be attributed to the absence (or poor preservation) of key taxa in some of the shallow-water lithofacies in the study area relative to more complete planktonic biotas preserved in basinal settings, or, perhaps, a result of provincialism of the calcareous nannoplankton and planktonic foraminifera. To resolve this issue, it will be necessary to study the Upper Cretaceous microfossil biostratigraphy in a much broader context, especially in the Middle East as outlined in this paper and recent work (e.g., Meilijson et al. 2014).

Absence of the early Coniacian CC13 and late Santonian *Calculites obscurus* (CC17) zones in all the studied sections indicates a major depositional hiatus at the Turonian/Coniacian, and Santonian/Campanian stage boundaries, respectively, throughout the region. These hiatuses are attributed to intra-plate deformation and regional tectonic uplift of the North African-Arabian Plates, part of the Late Cretaceous deformation of the Syrian Arc fold belt. Penecontemporaneous deformation and tilting of the depositional ramp was a major control on relative sea level and sedimention (chalk-chert-phosphorite association) on the mid- to inner-ramp from the Coniacian to Campanian, a period of major oceanic upwelling on the southern margin of Neo-Tethys. Lithofacies vary widely in the region from end-members of deeper-water pelagic chalk in the north to peritidal siliciclastics in the south. Lithofacies belts and their associated biofacies were dependent on their relative palaeogeographical position on the homoclinal ramp, with pelagic chalks and chalky marls, rich in calcareous nannofossils and planktonic foraminifera, deposited on the outer ramp (central and north Jordan); these lithofacies pass laterally to shallow-marine and peritidal siliciclastics in southeast Jordan and to the southwest in Egypt/Sinai. The flux of siliciclastic sediment into the basin was probably controlled by uplift of the mature Lower Palaeozoic and Lower Cretaceous sandstones of the Arabian Craton located to the southeast.

Four regional sequence boundaries (SB), some of which can be recognized globally, are marked by periods of depositional hiatus manifested at some boundaries by the absence of biozones (e.g. calcareous nannofossil zones CC13 (late Turonian) and CC17 (upper Santonian-earliest Campanian). Three sequence boundaries SB Tu/Co 1, SB Co/Sa 2 and SB Sa/Ca 3 are marked by local deformation and or depositional hiatuses characterised by bioerosion of hardground surfaces and/or encrusting benthic or endolithic faunas. These surfaces can be correlated throughout the region irrespective of lithologies and some show good correspondence with recently published Cretaceous sea-level curves. However, regional syn-tectonics (Syrian Arc deformation) resulted in local/regional relative sea-level changes (eurybatic shifts) on this sector of the north African-Arabian Platform.

Three deposition sequences (DS) have been recognized. TSTs are commonly marked by detrital (locally phosphatic chalk) in Jordan (basinwards) deposited during marine flooding of the pre-existing late Turonian rimmed carbonate platform (DS Eg/Jo1). HSTs are represented by hemi-pelagic chalk or chalk and marl. Lowstands are recognized by local emergence or bioerosion and encrustation of the sea floor and reduced sedimentation rates.

Acknowledgments We wish to express our gratitude to Prof. Maurice Tucker, and reviewers of Facies Journal for their helful comments which significantly improved the manuscript. John Powell publishes with the approval of the Executive Director, British Geological Survey (NERC).

References

Abed AM, Arouri KH, Boreham CJ (2005) Source rock potential of phosphorite-bituminous chalk-marl sequence in Jordan. Marine Petroleum Geology 22: 413-425

Abed, AM, Sadaqah R, Al-jazi M (2007) Sequence stratigraphy and evolution of Eshidiya phosphorite platform, southern Jordan. Sediment Geol 198:209-219

Abdel Gawad G I, El Sheikh HA, Abdelhamid MA, EL Beshtawy MK, Abed M, Fürsich FT (2004) Stratigraphic studies on some Upper Cretaceous succession in Sinai, Egypt. Egypt J Paleontol 4: 263-303

Abdel-Kireem MR, Samir AM, Ibrahim MI (1995) Upper Cretaceous planktonic foraminiferal zonation and correlation in the northern part of the Western Desert, Egypt. N Jb Geol Paläont Abh198: 329–361

Ahmad, F, Farouk, S, Abdel Moghny, MW (2014) A regional stratigraphic correlation for the upper Campanian phosphorites and associated rocks in Egypt and Jordan. P Geologists' Assoc 125: 419-431

Almogi-Labin A, Bein A, Sass E (1993) Late Cretaceous upwelling system along the southern Tethys margin (Israel): Interrelationship between productivity, bottom water environments, and organic matter preservation. Paleoceonography 8: 671-690

Al-Rifaiy, IA, Cherif OH, El-Bakri BA (1993) Upper Cretaceous foraminiferal biostratigraphy and paleobathymetry of the Al-Baqa area, North of Amman (Jordan). J Afri Earth Sci 7:343–357

Ardestani, SM, Vahidinia, M, Sadeghi, A, Arz, JA, Dochev D (2012) Integrated biostratigraphy of the Upper Cretaceous Abderaz Formation of the East Kopet Dagh Basin (NE Iran). Geol Balcanica 40 (1–3): 21–37

Attia, SH, Ismail, AA, Shabana, AR, Ismail, AA 2013 Contribution to the stratigraphy and sedimentation of the Cretaceous aquifers, SE Sinai, Egypt. Micropaleontology, 59: 177-200

Bachmann, M, Hirsch, F (2006) Lower Cretaceous carbonate platform of the eastern Levant (Galilee and the Golan Heights): stratigraphy and second-order sea-level change. Cret Res 27: 487-512

Bauer J, Kuss J, Steuber T (2002) Platform environments, microfacies and systems tracts of the upper Cenomanian-lower Santonian of Sinai, Egypt. Facies 47: 1–26.

Bauer, J, Kuss J, Steuber T (2003) Sequence architecture and carbonate platform configuration (Late Cenomanian-Santonian), Sinai, Egypt. Sedimentology 50/3: 387–414.

Bowen R, Jux, U (1987) Afro-Arabian geology. Chapman and Hall, London, 295p

Bralower TJ, Leckie RM, Sliter WV, Thierstein, H.R (1995) An integrated Cretaceous microfossil biostratigraphy. In: Berggren, WA, Kent, DV, Aubry, M-P, Hardenbol J (Eds.), Geochronology, Time Scales and Global Stratigraphic Correlation. SEPM Spec Publ 54:65-79

Bramlette MN, Sullivan FR (1961) Coccolithophorids and related nannoplankton of the Early Tertiary in California. Micropaleontology 7: 129-174

Burnett J A (with contribution from Gallagher L T, Hampton M J) (1998) Upper Cretaceous. In: Bown PR (ed) Calcareous Nannofossil Biostratigraphy, British Micropalaeontological Society Publication Series. London: Chapman and Hall/Kluwer Academic Publishers: 132-199

Caron M (1985) Cretaceous planktic foraminifera. In: Bolli, H.M., Saunders, J.B., Perch-Nielsen, K., (eds.), Plankton Stratigraphy. Cambridge University Press, Cambridge: 17-86

Chèrif OH, Al-Rifaiy IA, Al-Afifi FI, Orabi OH (1989) Planktonic foraminifera and chronostratigraphy of Senonian exposures in west-central Sinai, Egypt. Revue de Micropaléontol 32: 167–184

Cherif OH, Ismail AA (1991) Late Senonian-Tertiary planktonic foraminiferal biostratigraphy and tectonism of the Esh-el-Mallaha and Gharamul areas, Egypt. Middle East Research Center, Ain Shams University, E Sci Ser: 5: 146-159.

Coccioni R, Premoli Silva I (2015). Revised Upper Albian – Maastrichtian planktonic foraminiferal biostratigraphy and magneto-stratigraphy of the classical Tethyan Gubbio section (Italy). Newsl Stratigr 48: 47-90

Dunham RJ (1962) Classification of Carbonate Rocks According to Depositional Texture. In: Hamm WE, (ed.), Classification of Carbonate Rocks. Am Assoc Petrol Mem: 108-121

Elamri Z, Farouk S, Zaghbib-Turki D (2014). Santonian planktonic foraminiferal biostratigraphy of the northern Tunisia. Geologia Croatica 65/2:111-126.

El-Azabi MH, El-Araby A (2007). Depositional framework and sequence stratigraphic aspects of the Coniacian–Santonian mixed siliciclastic/carbonate Matulla sediments in Nezzazat and Ekma blocks, Gulf of Suez, Egypt. J Afr Earth Sci 47: 179–202

Embry AF, Klovan JE (1972) A late Devonian reef on North Easter Banks Island, northwest territories. Bul Can Petrol Gect 19: 730-781

Farouk S, Faris M (2012). Late Cretaceous Calcareous nannofossil and planktonic Foraminiferal bioevents of the shallow-marine Carbonate Platform in the Mitla Pass, west central Sinai, Egypt. Cret Res 33: 50-65

Farouk S (2014) Maastrichtian carbon cycle changes and planktonic foraminiferal bioevents at Gebel Matulla, west-central Sinai, Egypt. Cret Res 50: 238–251

Farouk S (2015) Upper Cretaceous sequence stratigraphy of the Galala Plateaux, western side of the Gulf of Suez, Egypt. MarPetrol Geology 60: 136-158

Fink J H, Reches Z (1983) Diagenetic density inversions and the deformation of shallow marine chert in Israel. Sedimentology 30: 261-271.

Flexer A, Rosenfield A, Lipson-Benitah S, Honigstein A (1986) Relative sea level changes during the Cretaceous in Israel. Am Assoc Petrol Geol Bull 70: 1685-1699

Flügel E (2004) Microfacies of Carbonate Rocks: Analysis, Interpretation and Application; Springer-Verlag, Berlin, 976p.

Freund RZ, Garfunkel Z, Zak I, Goldberg M, Weissbrod T, Derin B (1970). The shear along the Dead Sea rift. Phil Trans Royal Soc London 267A, p.107-130

Gale AS, Hancock JM, Kennedy WJ, Petrizzo MR, Lees JA, Walaszczyk I, Wray DS (2008) Geochemistry, stable oxygen and carbon isotopes, nannofossils, planktonic foraminifera, inoceramid bivalves, ammonites and crinoids of the Waxahachie Dam Spillway section, north Texas: a possible boundary stratotype for the base of the Campanian Stage. Cret Res29:131–167.

Ghorab MA, (1961) Abnormal stratigraphic features in Ras Gharib oil field. In: 3rd Arab Petroleum Congress, Alexandria, Egypt:10 pp.

Glenn CR, Arthur MA (1990) Anatomy and origin of a Cretaceous phosphorite-green sand giant, Egypt. Sedimentology 37: 123–148

Gradstein F M, Ogg J G, Schmitz M D, Ogg GM (2012). The Geologic Time-scale, First ed. Elsevier: 1176 pp.

Gruszczyňski M, Coleman M L, Marcinowski R, Walaszczyk I, Isaacs MCP (2002) Palaeoenvironmental conditions of hardgrounds formations in the Late Turonian-

Coniacian of Mangyshlak Mountains, Western Kazakhstan. Acta Geol. Pol. 52 (4): 423–435

Gvirtzman Z, Almogi-Labin A, Moshkovitz S, Lewy Z (1989) Upper Cretaceous high-resolution multiple stratigraphy, northern margin of the Arabian platform, central Israel. Cret Res 10: 107-135

Haq, BU (2014) Cretaceous eustasy revisited. Global and Planetary Change 113: 44–58

Haq BU, Al-Qahtani AM (2005) Phanerozoic cycles of sea-level change on the Arabian Platform. GeoArabia 10:127-160

Hardenbol J, Thierry J, Farley MB, Jacquin T, de Graciansky PC,Vail PR (1998) Mesozoic and Cenozoic sequence chronostratigraphic framework of European basins. In: de Graciansky P C, Hardenbol J, Jacquin T, Vail PR (eds.): Mesozoic and Cenozoic sequence stratigraphy of European Basins.SEPM Spec Publ 60: 3-13

Hay WW (1965) Calcareous nannofossils. In: Kummel B, Raup, D, (eds.) Handbook of paleontological techniques. Freeman, W.H., San Francisco, California, pp. 3-6.

Hermina M (1990) The surroundings of Kharga, Dakhla and Farafra oases. In: Said, R., (ed) The geology of Egypt. Balkema, Rotterdam/Brookfield pp. 259–292

Honigstein A, Almogi-Labin A, Rosenfeld A (1987) Combined ostracod and planktonic foraminiferal biozonation of the Late Coniacian-Earl Maastrichtian in Israel. Jl Micropalaeont 6:41-60.

Ismail AA, (2012) Late Cretaceous-Early Eocene benthic foraminifera from Esh El Mallaha area, Egypt. Rev Paléobiologie, Genève 31 (1): 15-50

Issawi B, Francis MH, Youssef EAA, Osman RA (2009) The Phanerozoic Geology of Egypt. In: Special Publication 81. The Egyptian Mineral Resource Authority. 589pp.Khalil H, Zahran E (2014) Calcareous Nannofossil Biostratigraphy and Stage Boundaries of the Santonian-Eocene Successions in Wadi El Mizeira Northeastern Sinai, Egypt. Inter JGeosc 5: 432-449

KochW (1968) Zurmikropaläontologie und biostratigraphie der Oberkreide und des Alttertiärs von Jordanien. Geol JBeihefte 85: 627-659

Kora M, Genedi A (1995). Lithostratigraphy and facies developmentof the Upper Cretaceous carbonates in east central Sinai, Egypt. Facies 32:223–236.

Kostic B, Aigner T (2004) Sedimentary and poroperm anatomy of shallow-water carbonates (Muschelkalk, South-German Basin): an outcrop analogue study of inter-well spacing scale. Facies 50: 113–131

Krenkel E (1924) Der Syriasche Bogen. Zen fur Mineral Geolog Palaontol 9: 274–281 (10: 301–313)

Kuss J (1986) Facies development of Upper Cretaceous-Lower Tertiary sediments of Monastery of St. Anthony, Eastern Desert, Egypt. Facies 15: 177–194

Kuss J, Christian Scheibner C, and Gietl R (2000) Carbonate Platform to Basin Transition along an Upper Cretaceous to Lower Tertiary Syrian Arc Uplift, Galala Plateau, Eastern Desert of Egypt. GeoArabia 5(3): 405-424.

La Maskin TA, Elrick M (1997) Sequence stratigraphy of the Middle to Upper Guilmette Formation, Southern Egan and Schell Creek Ranges, Nevada. In: Klapper G, Murphy, MA, Talent JA (eds.) Palaeozoic sequence stratigraphy, Biostratigraphy and Biogeography: Studies in Honor of J. Granville (ess) Johnson. Geol Soc Am Spec Paper 321: 89-112

Lamolda MA, Paul CRC, Peryt D, Pons JM (2014) The Global Bounadry Stratotype and Section Point (GSSP) for the base of the Santonian Stage, "Cantera de Margas", Olazagutia, northern Spain. Episodes: 37, 2-13

Lewy Z (1990) Transgressions, regressions and relative sea-level changes on the Cretaceous shelf of Israel and adjacent countries. A critical evaluation of Cretaceous global sea-level correlations. Paleoceanography 5:619-637

Lüning S, Kuss J, Bachmann M, Marzouk AM, Morsi AM (1998a) Sedimentary response to basin inversion: Mid Cretaceous Early Tertiary pre- to syndeformational deposition at the Arief El Naqa anticline (northern Sinai, Egypt). Facies 38: 103–136

Lüning S, Marzouk AM, Morsi A M, Kuss J (1998b) Sequence stratigraphy of the Upper Cretaceous of central-east Sinai, Egypt. Cret Res 19:153-196

Makhlouf, IM, Tarawneh K, Moumani K, Ibrahim K M (2015) Recognition of quartz geodes in the Upper Cretaceous Wadi Umm Ghudran Formation, Ras En Naqab, South Jordan. Arab J Geosci. 8: 1535-1547

McRae SG (1972). Glauconite. Earth Science Review 8:397–440

Meilijson A, Ashckenazi-Polivoda S, Ron-Yankovich L, Illner P, Alsenz H, Speijer R, Almogi-Labin A, Feinstein S, Berner Z, Püttmann W, Abramovich S (2014) Chronostratigraphy of the Upper Cretaceous high productivity sequence of the southern Tethys, Israel. Cret Res 50: 187-213

Mikbel S, Zacher W (1986) Fold structures in northern Jordan. N Jb Geol Paläont Mh 4: 248-256

Moh’d BK (2000) The Geology of Irbid and Ash Shuna Ash Shamaliyya (Waqqas) map sheets no. 3154-II and 3154-III. The Hashemite Kingdom of Jordan, Natural Resources Authority Bulletin 46, 63 (Amman)

Mustafa H (2000) Fish teeth from the Upper Umm Ghudran Formation (late Santonian) of NW-Jordan. N J Geol Paläont Mh10: 595-612

Mustafa H, Case G, Zalmout I (2002) A new selachian fauna from the Wadi Umm Ghudran Formation (Late Cretaceous)- Central Jordan. N Jb Geol Paläont Mh 226: 419-444.

Nederbragt AJ (1991) Late Cretaceous biostratigraphy and development of Heterohalicidae (planktic foraminifera): In: Biostratigraphy and paleoceanographic potential of Cretaceous planktic foraminifera Heterohelicidae– Centrale Huisdruk Kerj Vrije Uni ver siteit Amesterdam Academisch Proefschrift:, 61–125

Obaidalla NA, Kassab AS (2002) Integrated biostratigraphy of the Coniacian – Santonian sequence, southwestern Sinai, Egypt. Egypt J Paleont 2: 85-104

Ovechkina MN, Watkeys M, Mostovski MB (2009) Calcareous nannofossils from the stratotype section of the Mzamba Formation, Eastern Cape, South Africa. Palaeontol Afri 44: 129–133

Palma RM, Lazo DG, Piethé RD (2005) Facies de tormenta y trazas fósiles en la rampa media de la Formación La Manga, Bardas Blancas, Mendoza. Actas XVI Congreso Geológico Argentino, La Plata 3: 155-156

Parker DH (ed) (1970) The hydrogeology of the Mesozoic-Cainozoic aquifers of the western highlands and plateau of East Jordan. Investigation of the aquifers of east Jordan, Report of United Nations Development Project/Food and Agriculture Organization Project 212, Technical Report No. 2.Unpublished, Rome, 424 pp.

Perch-Nielsen, K (1985) Mesozoic Calcareous Nannofossils. In: Bolli HM, Saunders JB, Perch-Nielsen K (eds.), Plankton Stratigraphy, Cambridge Earth Sciences Series, Cambridge University Press, p.329–426

Petrizzo MR (2000) Upper Turonian-lower Campanian planktonic foraminifera from southern mid-high latitudes (Exmouth Plateau, NW Australia): biostratigraphy and taxonomic notes. Cret Res 21: 479–505.

Petrizzo MR (2002) Palaeoceanographic and palaeoclimatic inferences from Late Cretaceous planktonic foraminiferal assemblages from the Exmouth Plateau (ODP Sites 762 and 763, eastern Indian Ocean). Mar Micropaleontol 45: 117–150

Pettijohn FJ, Potter PE, Siever R (1987) Sand and Sandstones. Springer, New York, 553pp

Powell JH (1988) The geology of Karak. Map sheet No. 3152 III, NRA Geol Bull 8: pp 172. Amman

Powell JH (1989) Stratigraphy and Sedimentation of the Phanerozoic Rocks in Central and South Jordan - Part B: Kurnub, Ajlun and Belqa Groups. Geological Bulletin, No. 11.The Hashemite Kingdom of Jordan, Ministry of Energy and Mineral Resources, NRA Geol Bull, Amman, 130 pp

Powell JH, Moh'd BK (2011) Evolution of Cretaceous to Eocene alluvial and carbonate platform sequences in central and south Jordan. GeoArabia 16/4: 29–82

Powell JH, Moh'd, B K (2012) Early diagenesis of Late Cretaceous chalk-chert-phosphorite hardgrounds in Jordan: Implications for sedimentation on a Coniacian–Campanian pelagic ramp. GeoArabia 17/ 4: 17-38

Powell JH, Abed AM, Le Nindre Y-M (2014) Cambrian stratigraphy of Jordan. GeoArabia19: 81-134

Powers RW, Ramirez LF, Redmond CD, Elberg EL Jr (1966) Geology of the Arabian Peninsula: sedimentary geology of Saudi Arabia, US Geol Surv Prof Paper 560-D, 147 p

Premoli Silva I, Sliter WV (1995) Cretaceous planktonic foraminiferal biostratigraphy and evolutionary trends from the Bottaccione section, Gubbio, Italy. Palaeontogr Ital 82: 1–89

Premoli Silva I, Sliter W V (1999) Cretaceous paleoceanography: Evidence from planktonic foraminiferal evolution. Geol Soc America, Special Paper 332: 301–328

Pufahl PK, Grimm, KU, Abed AM, Sadaqah RMY (2003) Upper Cretaceous (Campanian) phosphorites in Jordan: implications for the formation of a southern Tethyan phosphorite giant. Sed Geol 161:175-205.

Razmjooei MJ, Thibault N, Kani1 A, Mahanipour A, Boussaha M, Korte C (2014) Coniacian–Maastrichtian calcareous nannofossil biostratigraphy and carbon-isotope stratigraphy in the Zagros Basin (Iran): consequences for the correlation of Late Cretaceous Stage Boundaries between the Tethyan and Boreal realms. Newsl Stratigr 47/2: 183–209

Reiss Z, Almogi-Labin A, Honigstein A, Lewy Z, Lipson-Benitah S, Moshkovitz S, Zaks Y (1985) Late Cretaceous multiple stratigraphic framework of Israel. Israel J Earth Sci 34:147–166

Robaszynski F, Caron M, Dupuis C, Amedro F, González-Donoso JM, Linares D, Hardenbol J, Gartner S, Calandra F, Deloffre R (1990) A tentative integrated stratigraphy in the Turonian of Central Tunisia: Formations, zones and sequential stratigraphy in the Kalaat Senan area. Bulletin des Centres de Recherches Exploration-Production Elf-Aquitaine 14: 213–384

Robaszynski F González-Donoso JM, Linares D, Amédro F, Caron M, Dupuis C, Dhondt AV, Gartner S (2000) Le Crétacé Supérieur de la région de Kalaat Senan, Tunisie centrale.

Litho-Biostratigraphy intégrée: zones d'ammonites, de foraminifères planctoniques et de nannofossiles du Turonien supérieur au Maastrichtien. Bulletin du Centre de Recherches, Exploration-Production Elf Aquitaine 22: 359–490

Samuel M, Ishmail A, Akarish A, Zaky A (2009) Upper Cretaceous stratigraphy of the Gebel Somar area, north-central Sinai, Egypt. Cret Res 30: 22-34

Sari B (2006) Upper Cretaceous planktonic foraminiferal biostratigraphy of the Bey Dağlari Autochthon in the Korkuteli area, Western Taurides, Turkey. J Foramin Res 36 (3): 241–261

Shahar J (1994) The Syrian Arc system: an overview. Palaeogeogr, Palaeoclimatol, Palaeoecol 112: 125–142

Shahin A, Kora M (1991) Biostratigraphy of some Upper Cretaceous successions in the Eastern Central Sinai, Egypt. N Jb Geol Paläont Mh 11: 671-692

Sharland PR, Archer R, Casey, DM, Davies, RB, Hall, SH, Heward, AP, Horbury A D, Simmons MD (2001) Arabian plate sequence stratigraphy. GeoArabia, Spec Publ 2:371 pp.

Sharland PR, Casey DM, Davies RB, Simmons, MD, Sutcliffe, OE (2004) Arabian Plate Sequence Stratigraphy–revisions to SP2. GeoArabia 9/1: 199-214

Sissingh W (1977) Biostratigraphy of Cretaceous calcareous nannoplankton .Geol. Mijnbouw 56: 37-65

Soudry D, Nathan Y, Roded R (1985) Ashosh-Haroz facies and their significance for the Mishash Formation paleogeography and phosphorite accumulation in the northern and central Negev, southern Israel. Israel Jn Earth Sci 56: 429–441

Stampfli G M, Borel G D (2002) A plate tectonic model for the Paleozoic and Mesozoic constrained by dynamic plate boundaries and restored synthetic oceanic isochrons: Earth Planet Sci Lett 196: 17–33

Steinitz G (1981) Enigmatic Chert Structures in the Senonian Cherts of Israel. Geol. Surv. Isr. Bull. 75:1-46.

Soudry D, Glenn CR, Nathan Y, Segal I, Vonder Haar D (2006) Evolution of Tethyan phosphogenesis along the northern edges of the Arabian-African shield during the Cretaceous-Eocene as deduced from temporal variations of Ca and Nd isotopes and rates of P accumulation. Earth-Sci Rev 78: 27-57

Tucker ME, Wright V P (1990) Carbonate Sedimentology: Oxford: Blackwell Scientific Publications, 482 p.

Voigt S, Gale AS, Jung C, Jenkyns HC (2012) Global correlation of Upper Campanian–Maastrichtian successions using carbon-isotope stratigraphy: development of a new Maastrichtian timescale. Newsl Stratigr 45:25–53

Walaszczyk I, Wood CJ, Lees JA, Peryt D, Voigt S, Wiese F (2010) The Salzgitter-Salder Quarry (Lower Saxony, Germany) and Słupia Nadbrżezna river cliff section (central Poland): a proposed candidate composite Global Boundary Stratotype Section and Point for the base of the Coniacian Stage (Upper Cretaceous). Acta Geol Pol 60: 445-477

Wanas HA (2008) Cenomanian rocks in the Sinai Peninsula, northeast Egypt: facies analysis and sequence stratigraphy. J Afr Earth Sci 52: 125–138

Warren J (2000) Dolomite: occurrence, evolution and economically important associations. Earth-Sci Rev 52: 1–81

Weiler Y, Sass E (1972) Karstic sandstone bodies in the Turonian limestones of Judea, Israel. Sediment Geol 7(2): 137-152

Wilson JL (1975) Carbonate Facies in Geological History. Springer-Verlag, Berlin. p. 471

Ziko A, Darwish M, Eweda S (1993). Late Cretaceous- Early Tertiary stratigraphy of the Themed area, East Central Sinai, Egypt. N Jb GeolPaläont Mh 13: 135-149

Figure caption

Fig. 1. Landsat image showing the location of the studied sections (Gebel Qabaliat, Gebel Nazazat, Ras el-Gifa sections in northeast Egypt; Karak, Wadi Mujib, and Wadi El-Ghafar in Jordan; source from Google Earth).

Fig. 2. Upper Cretaceous lithostratigraphical nomenclature, from south to north, in Egypt, Israel and Jordan

Fig. 3. Legend for figures in this paper

Fig. 4. Lithostratigraphical log of the Wadi Umm Ghudran Formation at three sections in Jordan (Karak, Wadi Mujib, and Wadi El-Ghafar) showing the biozones, facies associations, lateral and vertical facies, thickness variations and sequence stratigraphical interpretation (horizontal distance not to scale). Red lines represent the boundaries between the Mujib Chalk, Tafilah and Dhiban Chalk members. See Fig. 3 for legend and Table 1 for abbreviations of the microfacies.

Fig. 5. Lithostratigraphical log of the Matulla Formation (Gebel Qabaliat, Gebel Nazazat) and the equivalent Themed Formation (at Ras el-Gifa towards the north) in Egypt (Sinai)

showing the biozones, facies associations, lateral and vertical facies, thickness variations and sequence stratigraphic interpretation (horizontal distance not to scale). See Fig. 3 for legend and Table 1 for abbreviations of the microfacies.

Fig. 6A. General view of the exposed Upper Cretaceous succession at Wadi Mujib (south flank) showing the Naur Limestone, Fuheis, Hummar, Shueib, Wadi As Sir, Wadi Umm Ghudran, and Amman Silicified Limestone formations; the red lines indicate their boundaries; view to the southwest. (Field photograph: S. Farouk).

Fig. 6B. General view of the exposed Upper Cretaceous succession at Gebel Nazazat showing the Raha, Wata, Matulla, and Sudr Chalk formations; the red lines indicate their boundraies; view to north-west. Red dashed line separates the Lower Clastic Member from the overlying Middle Mixed Siliciclastic-Carbonate Member (Field photograph: S. Farouk).

Fig. 6C. The Tafilah Member unconformably underlies the Dhiban Chalk Member followed above unconformably by the Amman Silicified Limestone Formation with an irregular boundary; the red lines indicate their boundaries view to northwest. Car for scale ca. 1.5 m high (Field photograph: S. Farouk).

Fig.7. Coniacian to Campanian planktonic foraminiferal and calcareous nannofossil biostratigraphy of the studied sections compared to previous standard biostratigraphical schemes (Sissingh 1977; Perch-Nilsen 1985; Burnett 1998; Robaszynski et al. 2000) with stage boundaries of Gradstein et al. (2012).

Fig. 8. Distribution chart of the most important identified calcareous nannofossil and planktonic foraminiferal assemblages in the present study.

Fig. 9. Correlation chart showing the distribution of different hiatuses against the time-scale and standard zonation, with age of zonal boundaries according to the Gradstein et al. (2012) and Haq (2014) charts.

Fig. 10.

1- *Quadrum gartneri* Prins and Perch-Nielsen in Manivit et al. 1977, Wadi El-Ghafar section, Zone CC16.

2 -3- *Reinhardtites levis* Prins and Sissingh *in* Sissingh (1977), Karak section, Zone CC18.

4- *Broinsonia parca constricta* Hattner et al., 1980, Wadi Mujib section, Zone CC18.

5- *Prediscosphaera spinosa* (Bramlette & Marlini 1964) Gartner (1968), Ras el-Gifa section, Zone CC16.

6-*Arkhnangelskiella cymbiformis* Vekshina, Ras el-Gifa section, Zone CC18.

7- 8- *Eiffellithus eximius* (Stover 1966) Perch-Nielsen (1968), Wadi El-Ghafar section, Zone CC15.

9- *Eiffellithus turriseiffelii* (Deflandre *in* Deflandre & Fert 1954) Reinhardt 1965, Ras el-Gifa section, Zone CC15.

10- *Microrhabdulus decoratus* Deflandre (1959), Wadi Karak section, Zone CC16.

11- *Lucianorhabdus cayeuxii* Dellandre (1959), Mujib section, Zone CC15.

12- *Retecapsa crenulata* (Bramlette & Martini 1964) Grün *in* Grün and Allemann 1975, Wadi Karak section, Zone CC16.

13-16- *Watznaueria barnesae* (Black *in* Black & Barnes 1959) Perch-Nielsen (1968), Wadi Mujib section, Zone CC18.

Fig. 11

1-4: *Heterohelix globulosa* (Eherenbeg 1840), Wadi El-Ghafar section, *Dicarinella asymetrica*

Zone.

5: *Costellagerina bulbosa* (Belford 1960), Ras el-Gifa section, *Dicarinella asymetrica* Zone.

6: *Costellagerina* cf. *pilula* (Belford 1960), Wadi El-Ghafar section, *Dicarinella asymetrica* Zone.

7-9: *Dicarinella asymetrica* (Sigal 1952), Wadi El-Ghafar section, *Globotruncanita elevata* Zone.

10-11: *Dicarinella* sp., Ras el-Gifa section, *Dicarinella asymetrica* Zone.

12-13: *Marginotruncana sinuosa* Porthault 1970, Wadi El-Ghafar section, *Globotruncanita elevata Zone.*

14-15: *Globotruncana arca* (Cushman 1926), Wadi El-Ghafar section, *Globotruncanita elevata* Zone.

16-17: *Globotruncana bulloides* Vogler 1941, Wadi El-Ghafar section, *Globotruncanita elevata* Zone.

18: *Globotruncana linneiana* (D'orbigny 1839), Wadi El-Ghafar section, *Globotruncanita elevata* Zone.

Fig. 12: Microfacies of Coniacian-Santonian successions in northeast Egypt and Jordan. Scale bar = 200 µm. A) FT2, calcareous glauconitic quartz arenite; sample 32, Gebel Qabaliat section. B) FT3, quartz arenite; sample 41, Gebel Qabaliat section. C) FT4, sandy evaporitic recrystallized lime-mudstone; sample 41, Gebel Qabaliat section. D) FT5, ferruginous sandy dolomicrite; sample 79 section, Gebel Nazazat section. E) FT9, recrystallized sandy dolomicrite; sample 50, Gebel Qabaliat section. F) FT10, phosphatic glauconitic sandy lime-mudstone; sample 49, Gebel Qabaliat section. G) FT11, Serpulid bioclastic wacke/packstone; sample 48, Gebel Qabaliat section. H) FT12, Well-bedded

chert interbedded with limestone; sample 84, Mujib section. I) FT13, onco-ooidal-packstone; sample 19, Ras el-Gifa section

Fig. 13: Microfacies of Coniacian-Santonian successions in northeast Egypt and Jordan. Scale bar = 200 µm. A) FT14, glauconitic peloidal packstone; sample 23, Ras el-Gifa section. B) FT18, bioclastic packstone; sample 10, Ras el-Gifa section. C) FT21, oncoidal bioclastic wacke/packstone; sample 21, Ras el-Gifa section. D) FT22, glauconitic sandy bioclastic wackestone; sample 45, Gebel Qabaliat section. E) FT23, oyster glauconitic floatstone; sample 47, Gebel Qabaliat section. F & G) FT24, bio – intraclastic sandy packstone; sample 141, Karak section. H & I) FT26, planktonic foraminiferal wackestone; the rock contains sponge spicules with some yellow silicification of glauconite, sample 33, Wadi El-Ghafar section.

Fig. 14. Block diagram showing the distribution of the sedimentary lithofacies for the Coniacian - Santonian succession in the study area, from south to north. See Fig. 3 for legend.

Fig. 15. Correlation of sequence boundaries in different regions of the Arabian platform, Egypt and Jordan, and the revised eustatic Cretaceous sea-level changes of Haq (2014); timescale after Gradstein et al. (2012).

Fig. 16. Correlation chart of the Coniacian-Santonian sequences showing the facies associations, and sequence stratigraphic interpretation in the studied sections (horizontal distance not to scale). See Fig. 3 for legend.

Table 1 Facies types recognized in the present study.

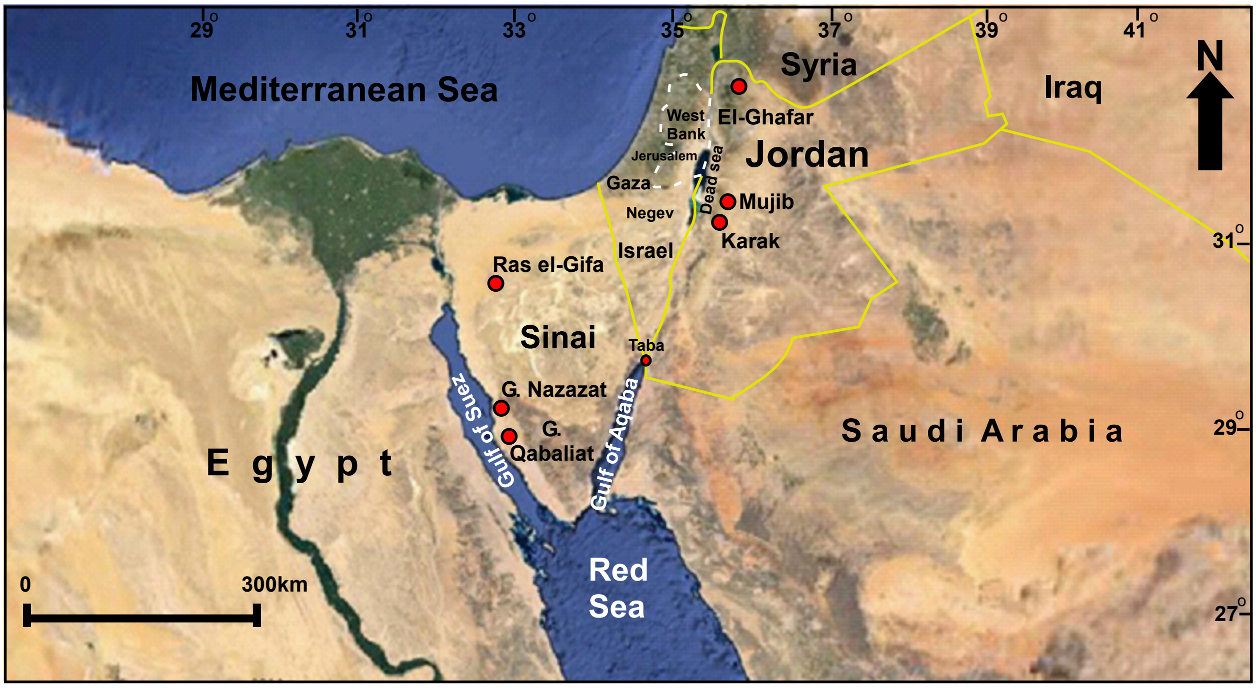
29°
31°
33°
35°
37°
39°
41°
Mediterranean Sea
Syria
Iraq
N
West Bank
El-Ghafar
Jerusalem
Dead sea
Jordan
Gaza
Mujib
Negev
Karak
31°
Israel
Ras el-Gifa
Sinai
Taba
G. Nazazat
Gulf of Suez
G. Qabaliat
Gulf of Aqaba
Saudi Arabia
29°
Egypt
Red Sea
0
300km
27°

Fig. 1

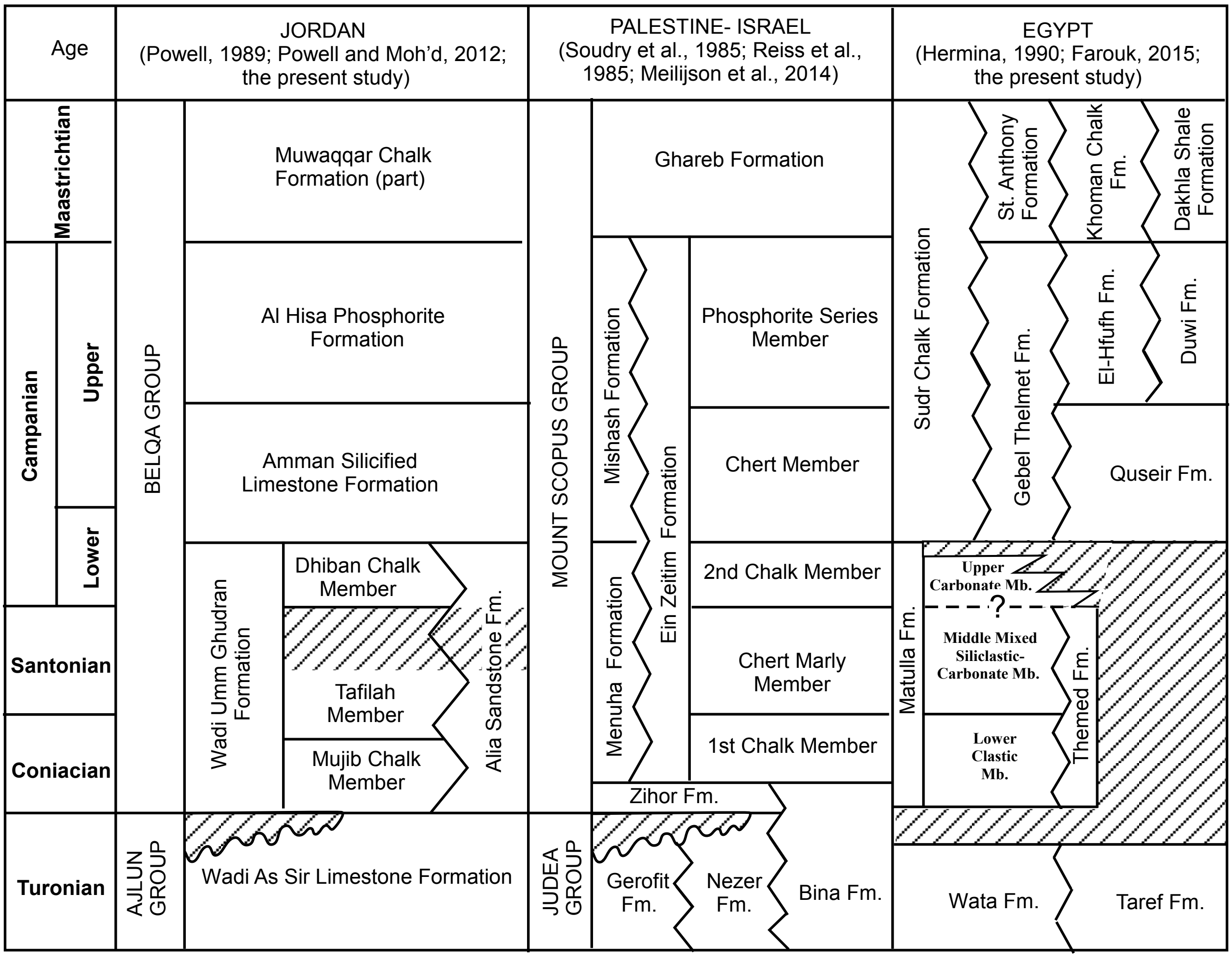
Age
JORDAN
(Powell, 1989; Powell and Moh'd, 2012; the present study)
PALESTINE- ISRAEL
(Soudry et al., 1985; Reiss et al., 1985; Meilijson et al., 2014)
EGYPT
(Hermina, 1990; Farouk, 2015; the present study)
Maastrichtian
Campanian
Upper
Lower
Santonian
Coniacian
Turonian
BELQA GROUP
AJLUN GROUP
Muwaqqar Chalk Formation (part)
Al Hisa Phosphorite Formation
Amman Silicified Limestone Formation
Wadi Umm Ghudran Formation
Dhiban Chalk Member
Tafilah Member
Mujib Chalk Member
Alia Sandstone Fm.
Wadi As Sir Limestone Formation
MOUNT SCOPUS GROUP
JUDEA GROUP
Ghareb Formation
Mishash Formation
Menuha Formation
Ein Zeitim Formation
Phosphorite Series Member
Chert Member
2nd Chalk Member
Chert Marly Member
1st Chalk Member
Zihor Fm.
Gerofit Fm.
Nezer Fm.
Bina Fm.
Sudr Chalk Formation
St. Anthony Formation
Khoman Chalk Fm.
Dakhla Shale Formation
Gebel Thelmet Fm.
El-Hfufh Fm.
Duwi Fm.
Quseir Fm.
Matulla Fm.
Upper Carbonate Mb.
?
Middle Mixed Siliclastic-Carbonate Mb.
Lower Clastic Mb.
Themed Fm.
Wata Fm.
Taref Fm.

Fig. 2

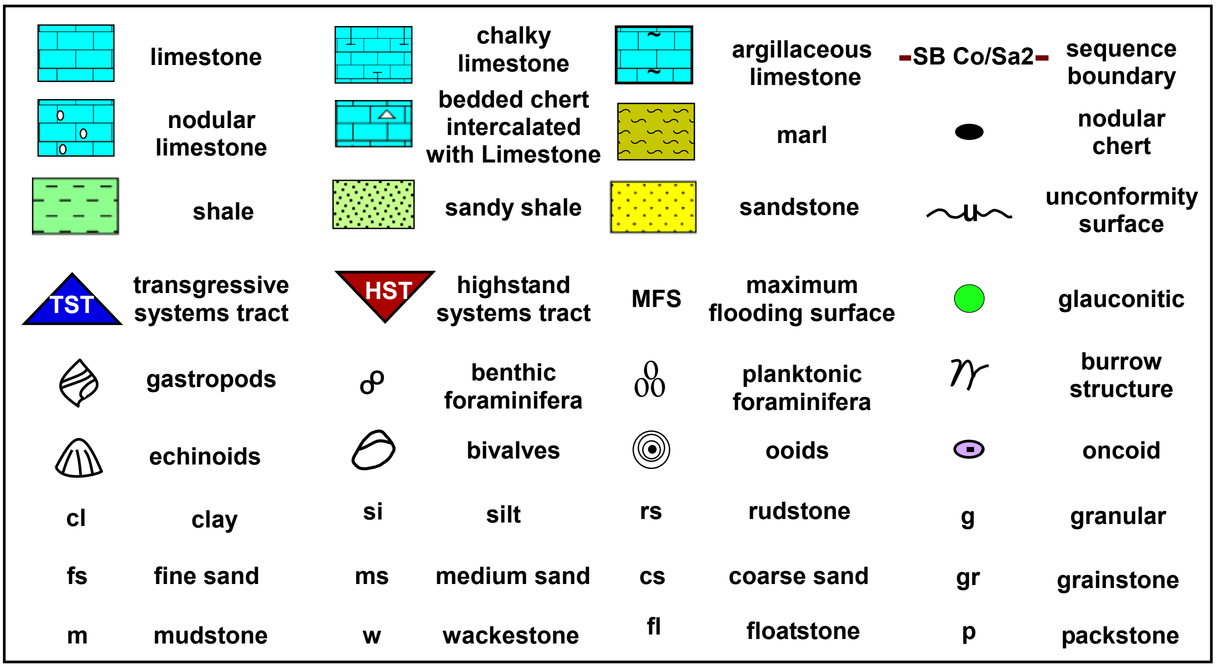
limestone
chalky limestone
argillaceous limestone
SB Co/Sa2
sequence boundary
nodular limestone
bedded chert intercalated with Limestone
marl
nodular chert
shale
sandy shale
sandstone
unconformity surface
TST
transgressive systems tract
HST
highstand systems tract
MFS
maximum flooding surface
glauconitic
gastropods
benthic foraminifera
planktonic foraminifera
burrow structure
echinoids
bivalves
ooids
oncoid
cl
clay
si
silt
rs
rudstone
g
granular
fs
fine sand
ms
medium sand
cs
coarse sand
gr
grainstone
m
mudstone
w
wackestone
fl
floatstone
p
packstone

Fig. 3

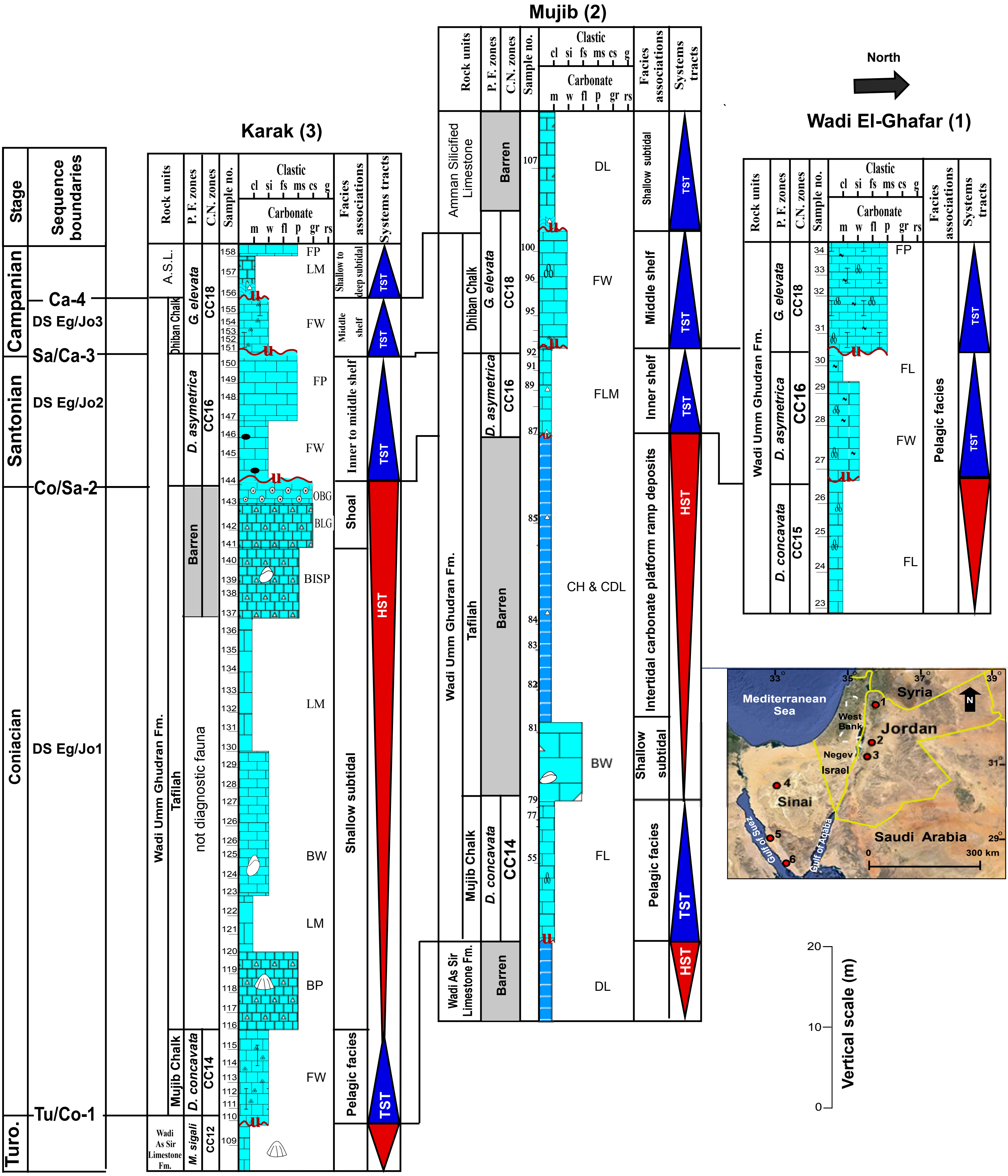

Karak (3)
Mujib (2)
Wadi El-Ghafar (1)
North
Stage
Sequence boundaries
Campanian
Santonian
Coniacian
Turo.
Ca-4
DS Eg/Jo3
Sa/Ca-3
DS Eg/Jo2
Co/Sa-2
DS Eg/Jo1
Tu/Co-1
Rock units
P. F. zones
C.N. zones
Sample no.
Clastic
cl si fs ms cs g
Carbonate
m w fl p gr rs
Facies associations
Systems tracts
A.S.L.
Dhiban Chalk
Wadi Umm Ghudran Fm.
Tafilah
Mujib Chalk
Wadi As Sir Limestone Fm.
Amman Silicified Limestone
G. elevata
D. asymetrica
D. concavata
M. sigali
CC18
CC16
CC15
CC14
CC12
Barren
not diagnostic fauna
FP
LM
FW
OBG
BLG
BISP
BW
BP
DL
FLM
CH & CDL
FL
Shallow to deep subtidal
Middle shelf
Inner to middle shelf
Shoal
Shallow subtidal
Pelagic facies
Inner shelf
Intertidal carbonate platform ramp deposits
TST
HST
Mediterranean Sea
West Bank
Negev
Israel
Sinai
Syria
Jordan
Saudi Arabia
Gulf of Suez
Gulf of Aqaba
N
300 km
Vertical scale (m)

Fig. 4

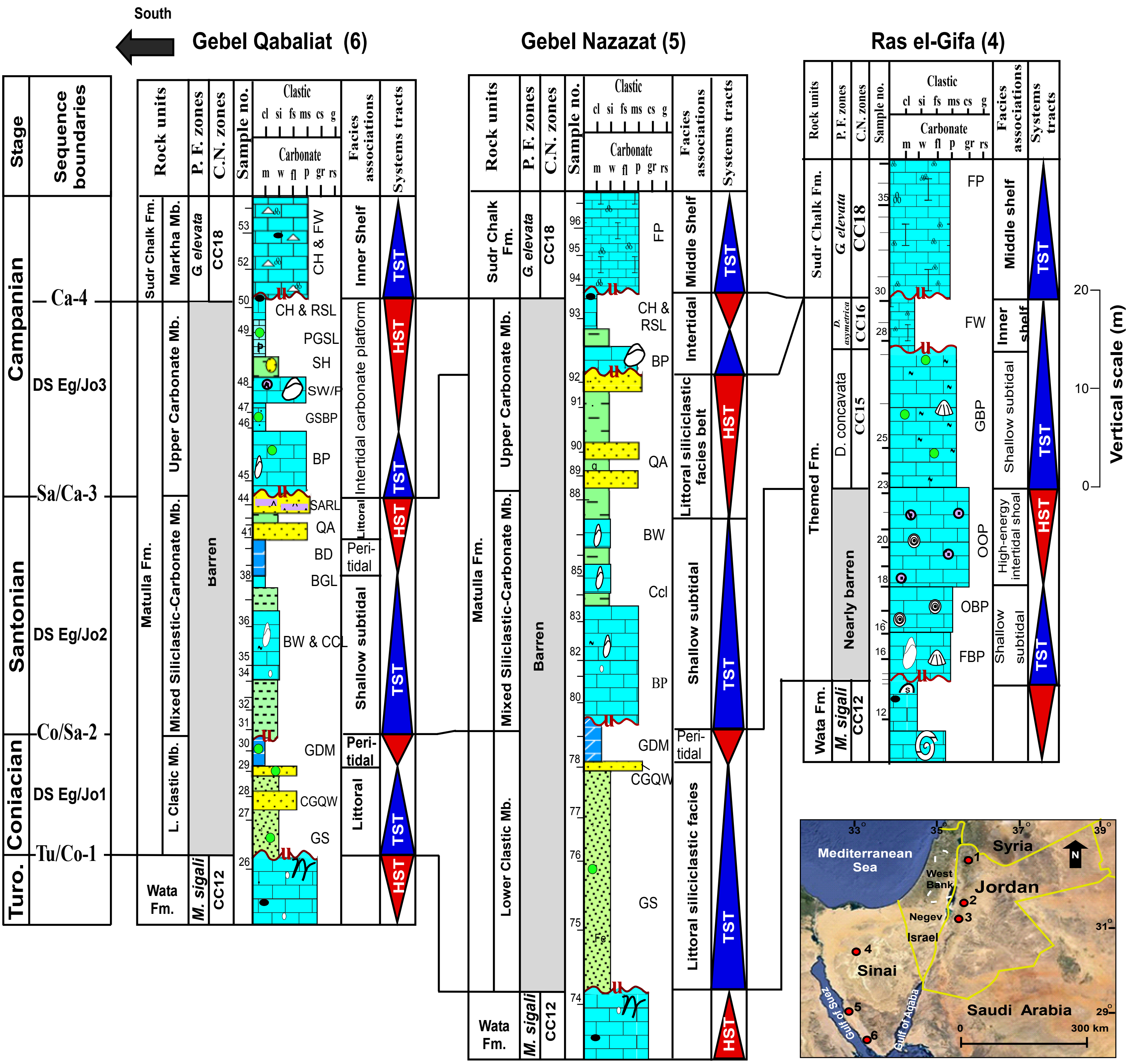
South
Gebel Qabaliat (6)
Gebel Nazazat (5)
Ras el-Gifa (4)
Stage
Sequence boundaries
Rock units
P. F. zones
C.N. zones
Sample no.
Clastic
Carbonate
Facies associations
Systems tracts
Campanian
Santonian
Coniacian
Turo.
Ca-4
Sa/Ca-3
Co/Sa-2
Tu/Co-1
DS Eg/Jo3
DS Eg/Jo2
DS Eg/Jo1
Sudr Chalk Fm.
Markha Mb.
Matulla Fm.
Upper Carbonate Mb.
Mixed Siliciclastic-Carbonate Mb.
L. Clastic Mb.
Lower Clastic Mb.
Wata Fm.
Themed Fm.
Barren
Nearly barren
G. elevata
D. asymetrica
D. concavata
M. sigali
CC18
CC16
CC15
CC12
CH & FW
CH & RSL
PGSL
SH
SW/P
GSBP
BP
SARL
QA
BD
BGL
BW & CCL
GDM
CGQW
GS
FP
BW
Ccl
FW
GBP
OOP
OBP
FBP
Inner Shelf
Intertidal carbonate platform
Littoral
Peri-tidal
Shallow subtidal
Middle Shelf
Intertidal
Littoral siliciclastic facies belt
Littoral siliciclastic facies
Middle shelf
Inner shelf
High-energy intertidal shoal
TST
HST
Vertical scale (m)
Mediterranean Sea
Syria
Jordan
West Bank
Negev
Israel
Sinai
Saudi Arabia
Gulf of Suez
Gulf of Aqaba
300 km

Fig. 5

A

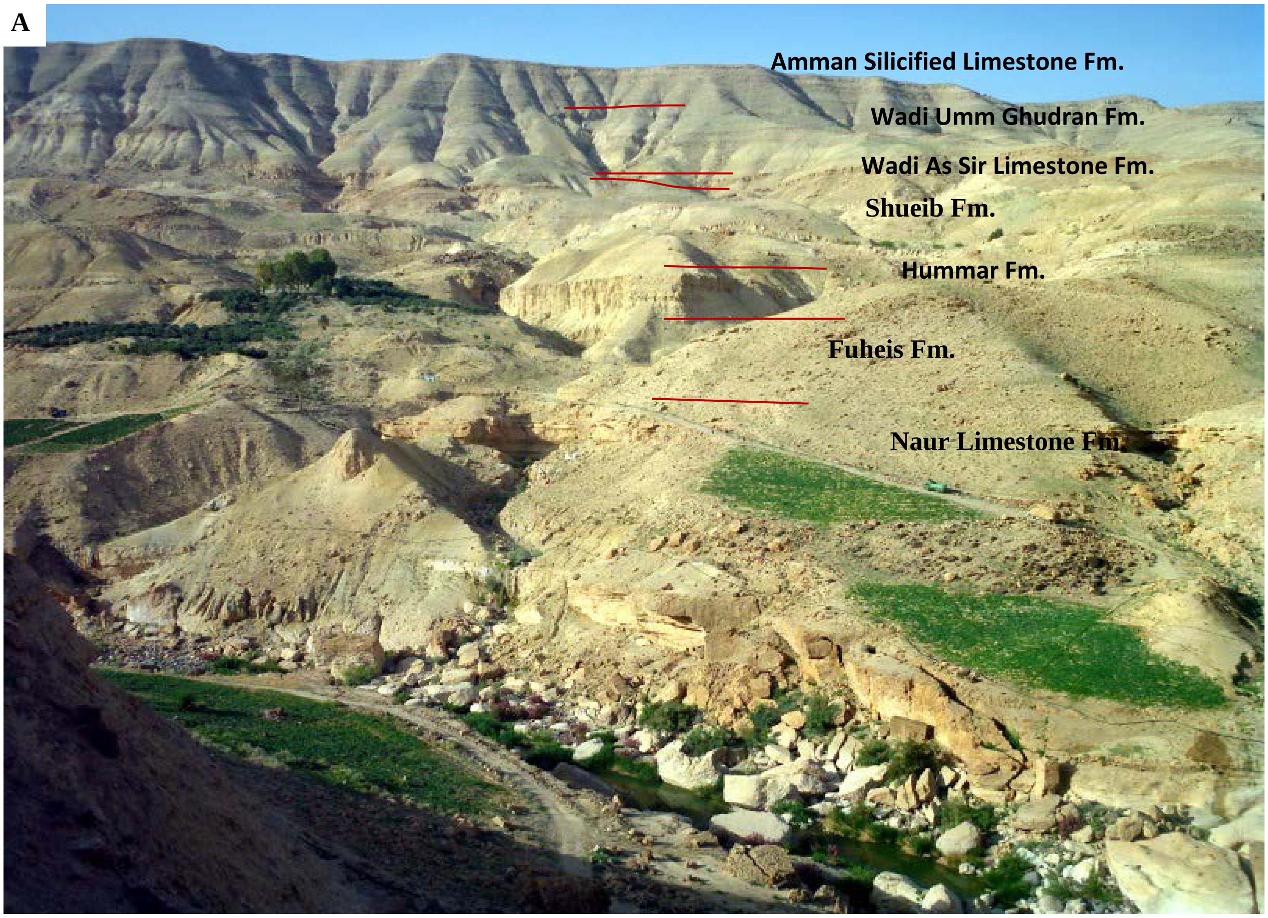
Amman Silicified Limestone Fm.
Wadi Umm Ghudran Fm.
Wadi As Sir Limestone Fm.
Shueib Fm.
Hummar Fm.
Fuheis Fm.
Naur Limestone Fm.

B

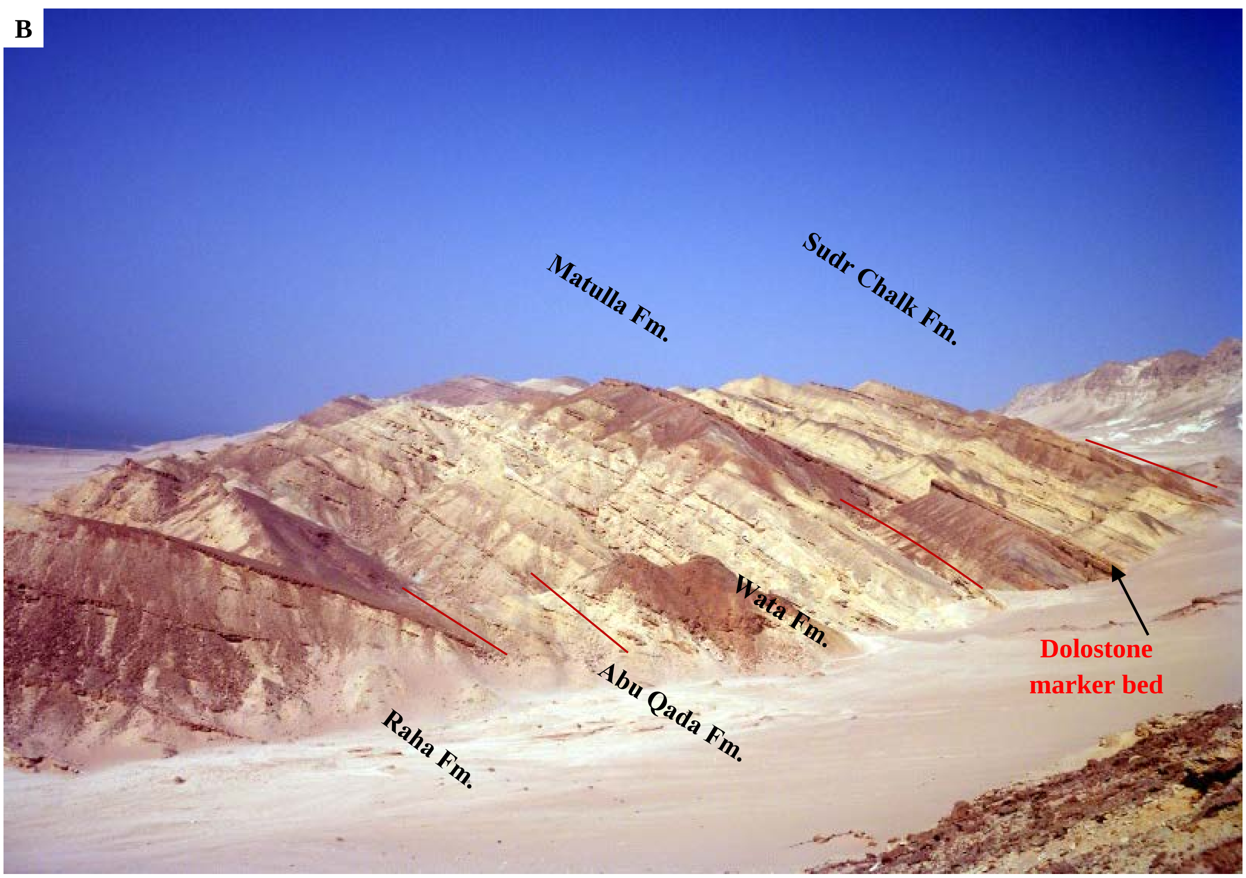
Matulla Fm.
Sudr Chalk Fm.
Wata Fm.
Dolostone
marker bed
Abu Qada Fm.
Raha Fm.

C

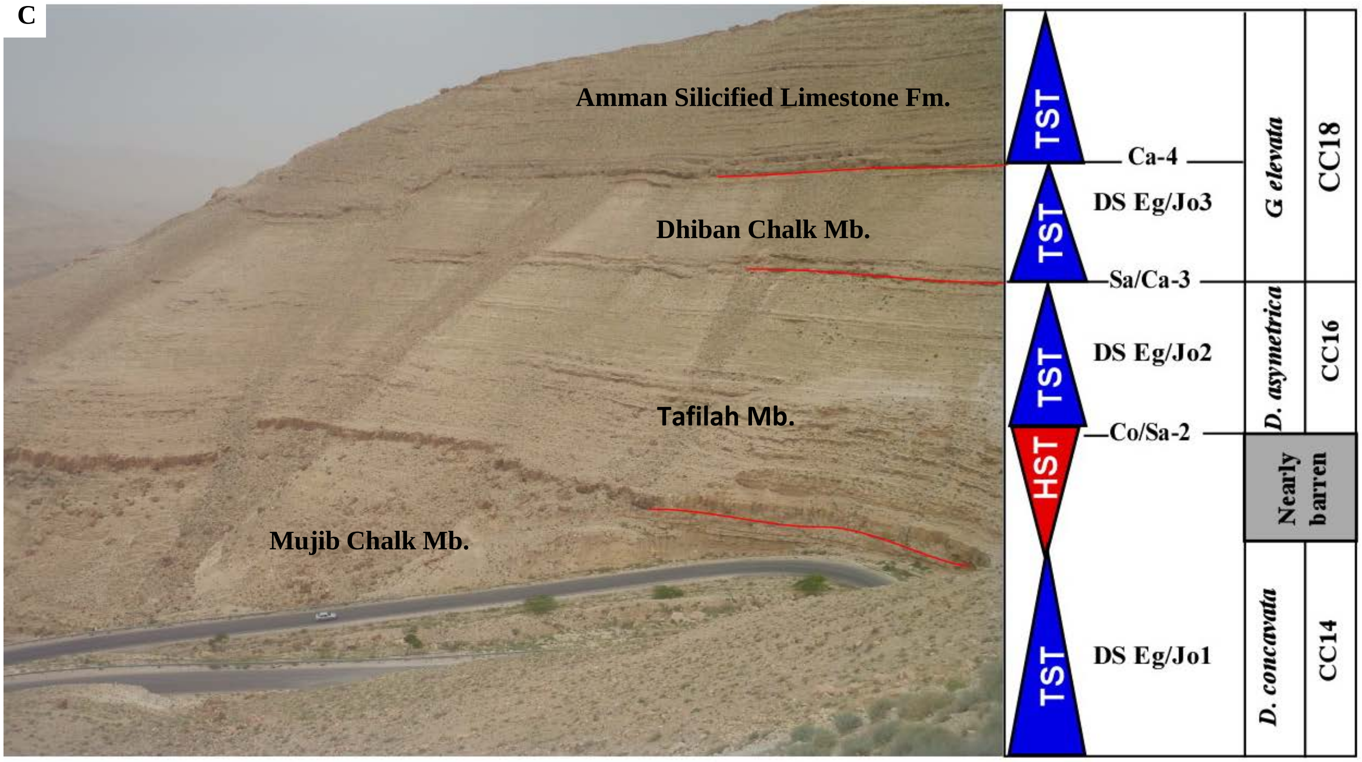

Amman Silicified Limestone Fm.
Dhiban Chalk Mb.
Tafilah Mb.
Mujib Chalk Mb.
TST
Ca-4
DS Eg/Jo3
TST
Sa/Ca-3
DS Eg/Jo2
TST
Co/Sa-2
HST
DS Eg/Jo1
TST
G elevata
CC18
D. asymetrica
CC16
Nearly barren
D. concavata
CC14

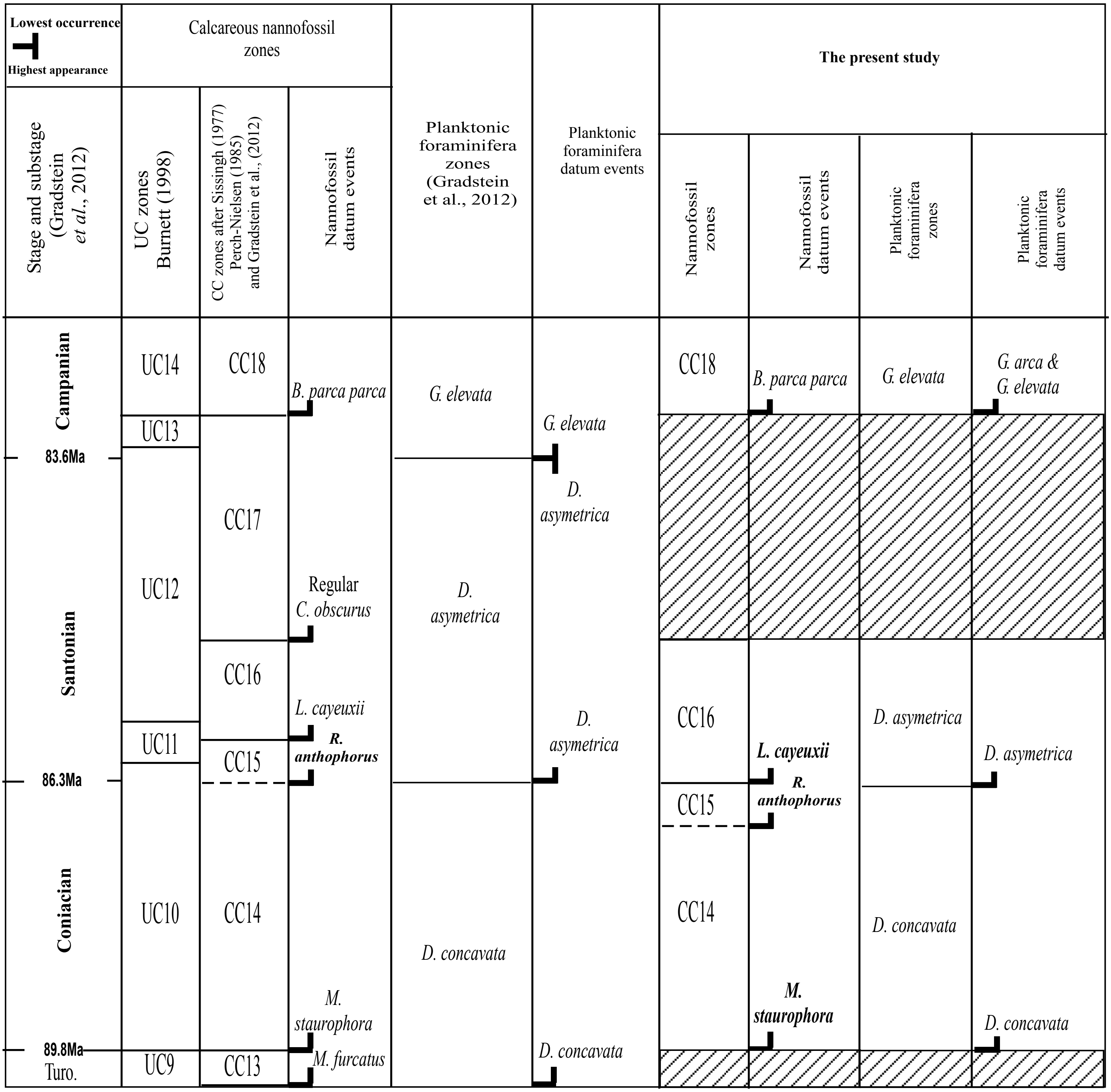
Lowest occurrence
Highest appearance
Calcareous nannofossil zones
The present study
Stage and substage (Gradstein et al., 2012)
UC zones Burnett (1998)
CC zones after Sissingh (1977) Perch-Nielsen (1985) and Gradstein et al., (2012)
Nannofossil datum events
Planktonic foraminifera zones (Gradstein et al., 2012)
Planktonic foraminifera datum events
Nannofossil zones
Nannofossil datum events
Planktonic foraminifera zones
Planktonic foraminifera datum events
Campanian
Santonian
Coniacian
Turo.
83.6Ma
86.3Ma
89.8Ma
UC14
UC13
UC12
UC11
UC10
UC9
CC18
CC17
CC16
CC15
CC14
CC13
B. parca parca
Regular C. obscurus
L. cayeuxii
R. anthophorus
M. staurophora
M. furcatus
G. elevata
D. asymetrica
D. concavata
G. elevata
D. asymetrica
D. asymetrica
D. concavata
CC18
CC16
CC15
CC14
B. parca parca
L. cayeuxii
R. anthophorus
M. staurophora
G. elevata
D. asymetrica
D. concavata
G. arca & G. elevata
D. asymetrica
D. concavata

Fig. 7

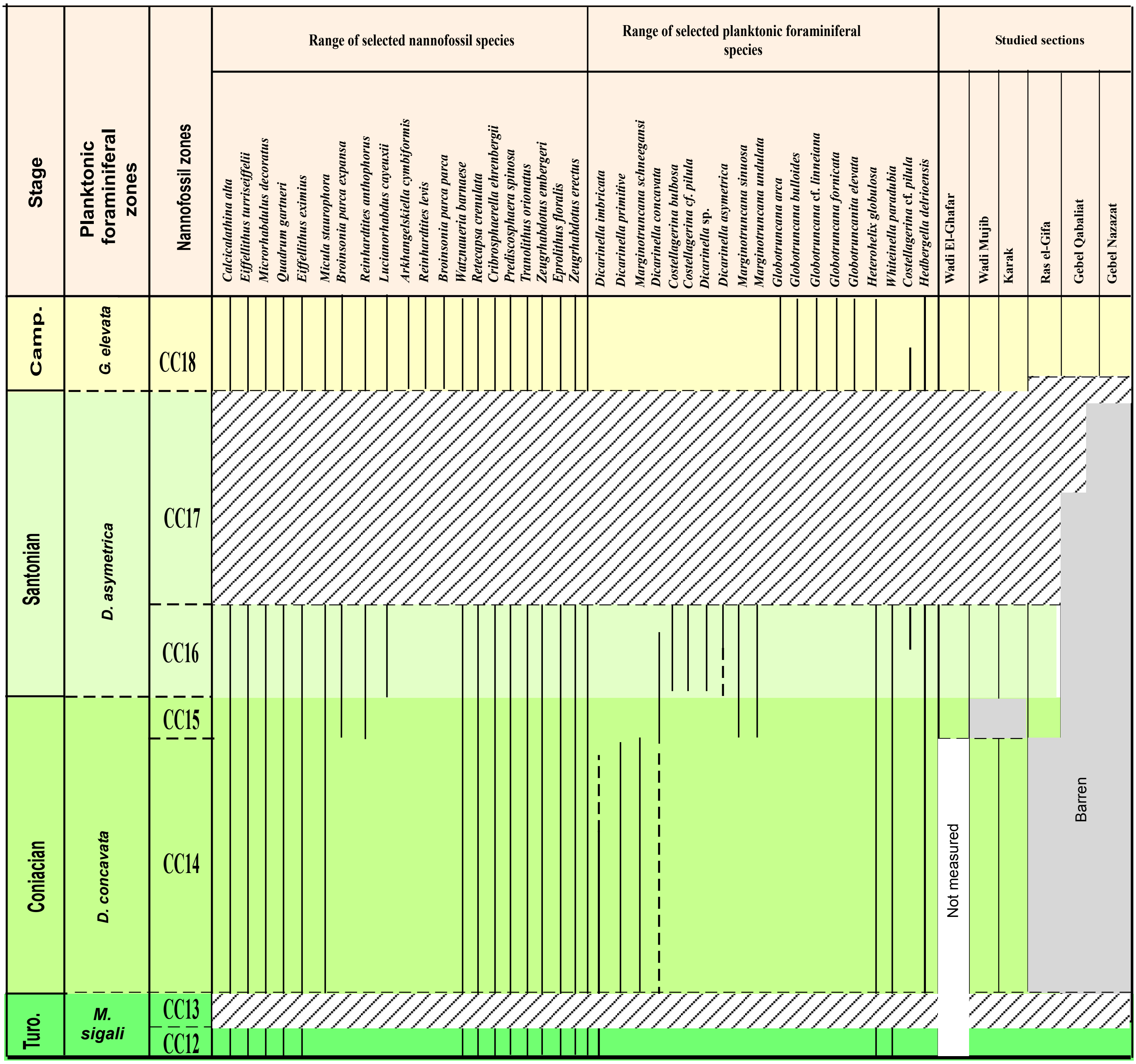

Stage
Planktonic foraminiferal zones
Nannofossil zones
Range of selected nannofossil species
Range of selected planktonic foraminiferal species
Studied sections
Calcicalathina alta
Eiffellithus turriseiffelii
Microrhabdulus decoratus
Quadrum gartneri
Eiffellithus eximius
Micula staurophora
Broinsonia parca expansa
Reinhardtites anthophorus
Lucianorhabdus cayeuxii
Arkhangelskiella cymbiformis
Reinhardtites levis
Broinsonia parca parca
Watznaueria barnaese
Retecapsa crenulata
Cribrosphaerella ehrenbergii
Prediscosphaera spinosa
Tranolithus orionatus
Zeugrhabdotus embergeri
Eprolithus floralis
Zeugrhabdotus erectus
Dicarinella imbricata
Dicarinella primitive
Marginotruncana schneegansi
Dicarinella concavata
Costellagerina bulbosa
Costellagerina cf. pilula
Dicarinella sp.
Dicarinella asymetrica
Marginotruncana sinuosa
Marginotruncana undulata
Globotruncana arca
Globotruncana bulloides
Globotruncana cf. linneiana
Globotruncana fornicata
Globotruncanita elevata
Heterohelix globulosa
Whiteinella paradubia
Costellagerina cf. pilula
Hedbergella delrioensis
Wadi El-Ghafar
Wadi Mujib
Karak
Ras el-Gifa
Gebel Qabaliat
Gebel Nazazat
Camp.
G. elevata
CC18
Santonian
D. asymetrica
CC17
CC16
Coniacian
D. concavata
CC15
CC14
Turo.
M. sigali
CC13
CC12
Not measured
Barren

Fig. 8

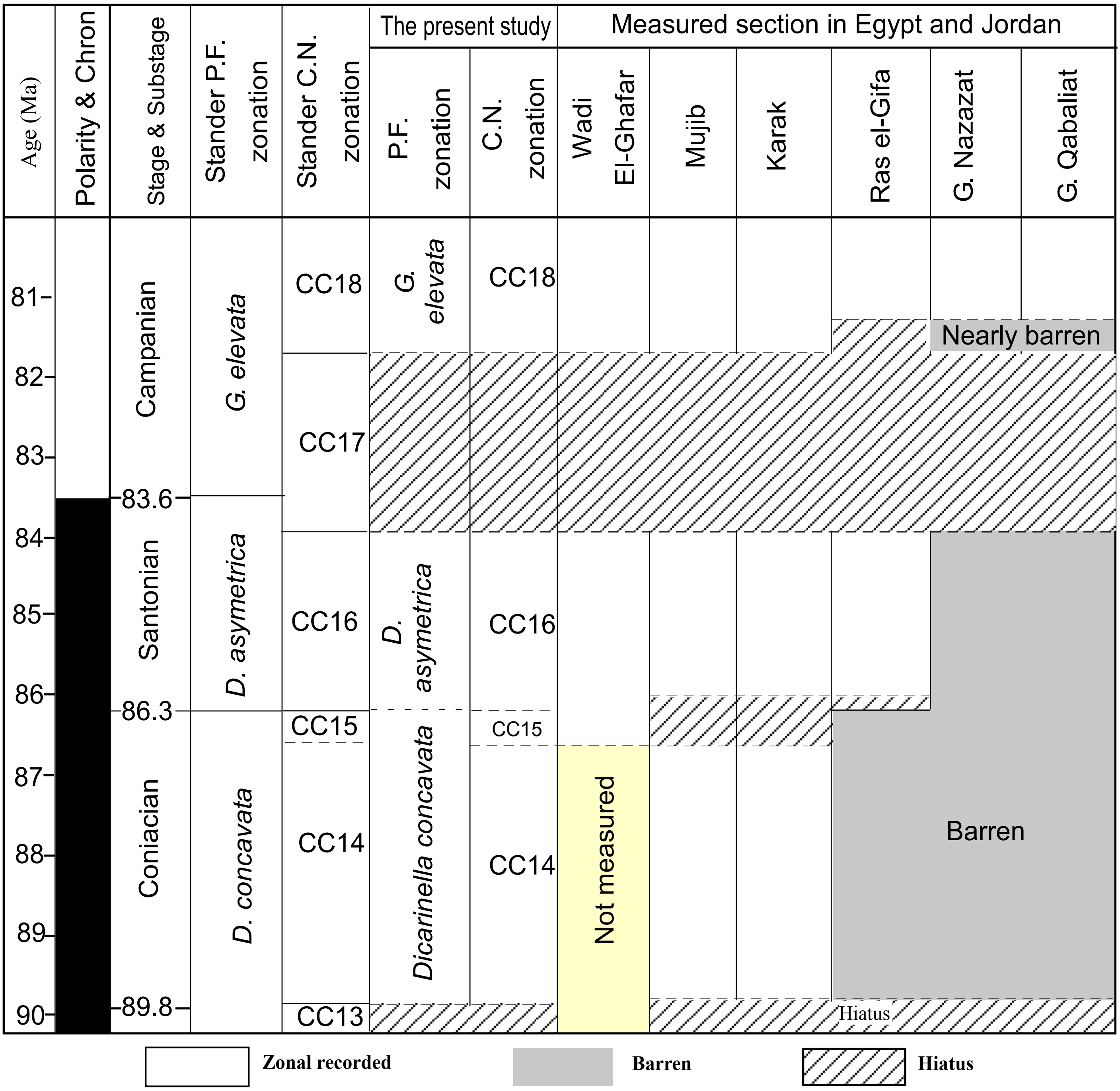

Age (Ma)
Polarity & Chron
Stage & Substage
Stander P.F. zonation
Stander C.N. zonation
The present study
P.F. zonation
C.N. zonation
Measured section in Egypt and Jordan
Wadi El-Ghafar
Mujib
Karak
Ras el-Gifa
G. Nazazat
G. Qabaliat
81
82
83
84
85
86
87
88
89
90
83.6
86.3
89.8
Campanian
Santonian
Coniacian
G. elevata
D. asymetrica
D. concavata
CC18
CC17
CC16
CC15
CC14
CC13
G. elevata
D. asymetrica
Dicarinella concavata
CC18
CC16
CC15
CC14
Nearly barren
Not measured
Barren
Hiatus
Zonal recorded
Barren
Hiatus

Fig. 9

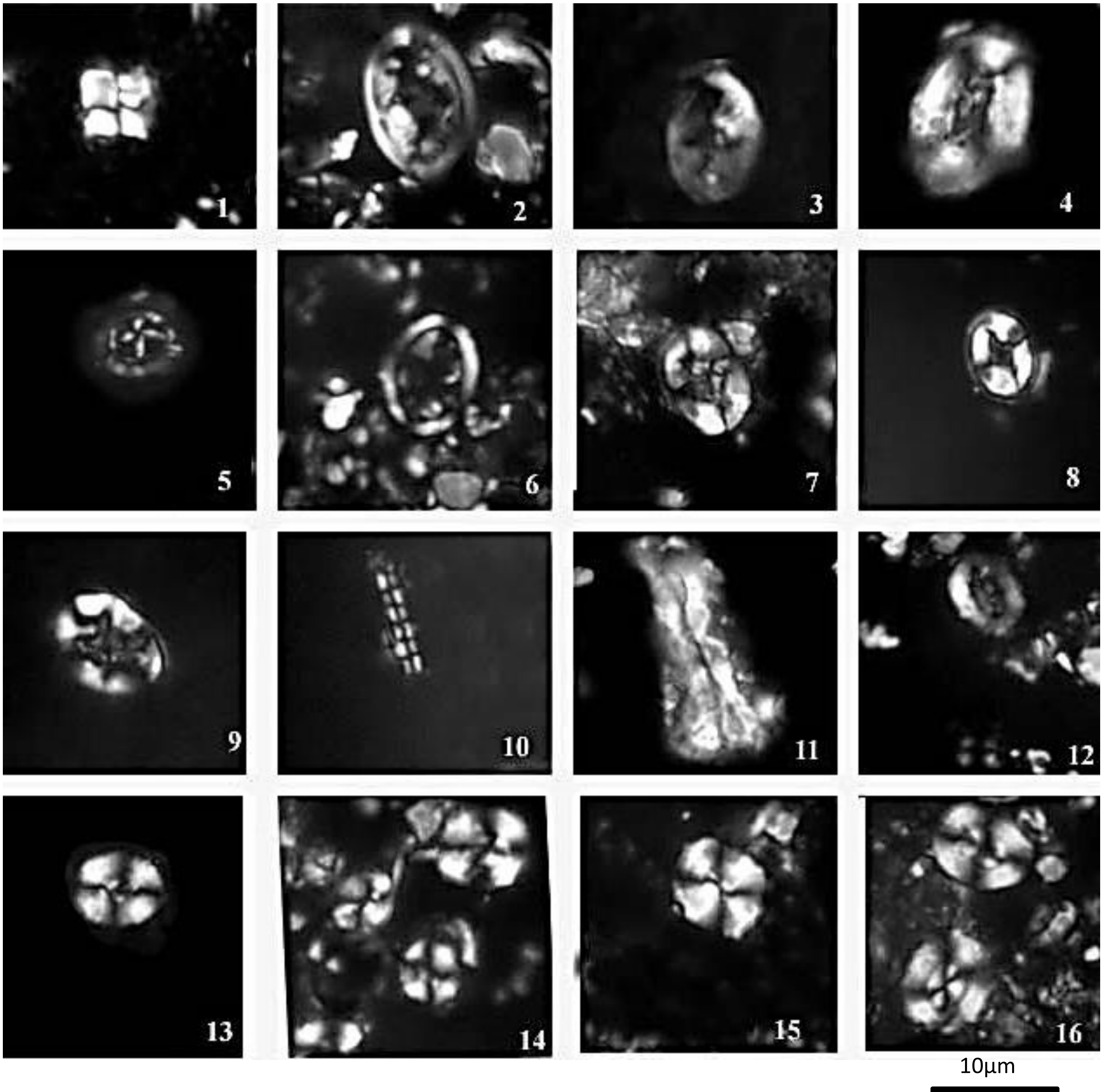

Fig. 10

Fig. 11

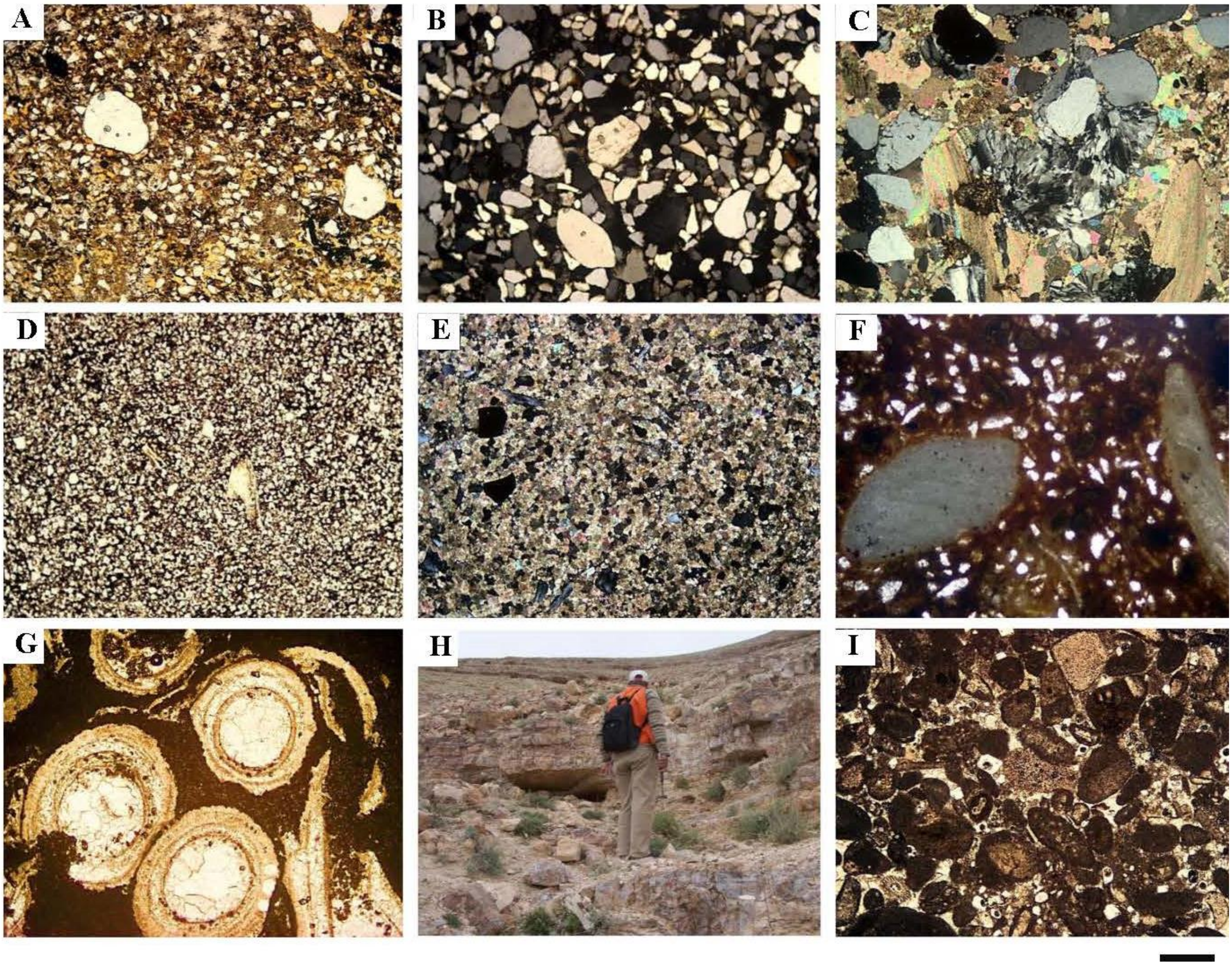

Fig. 12

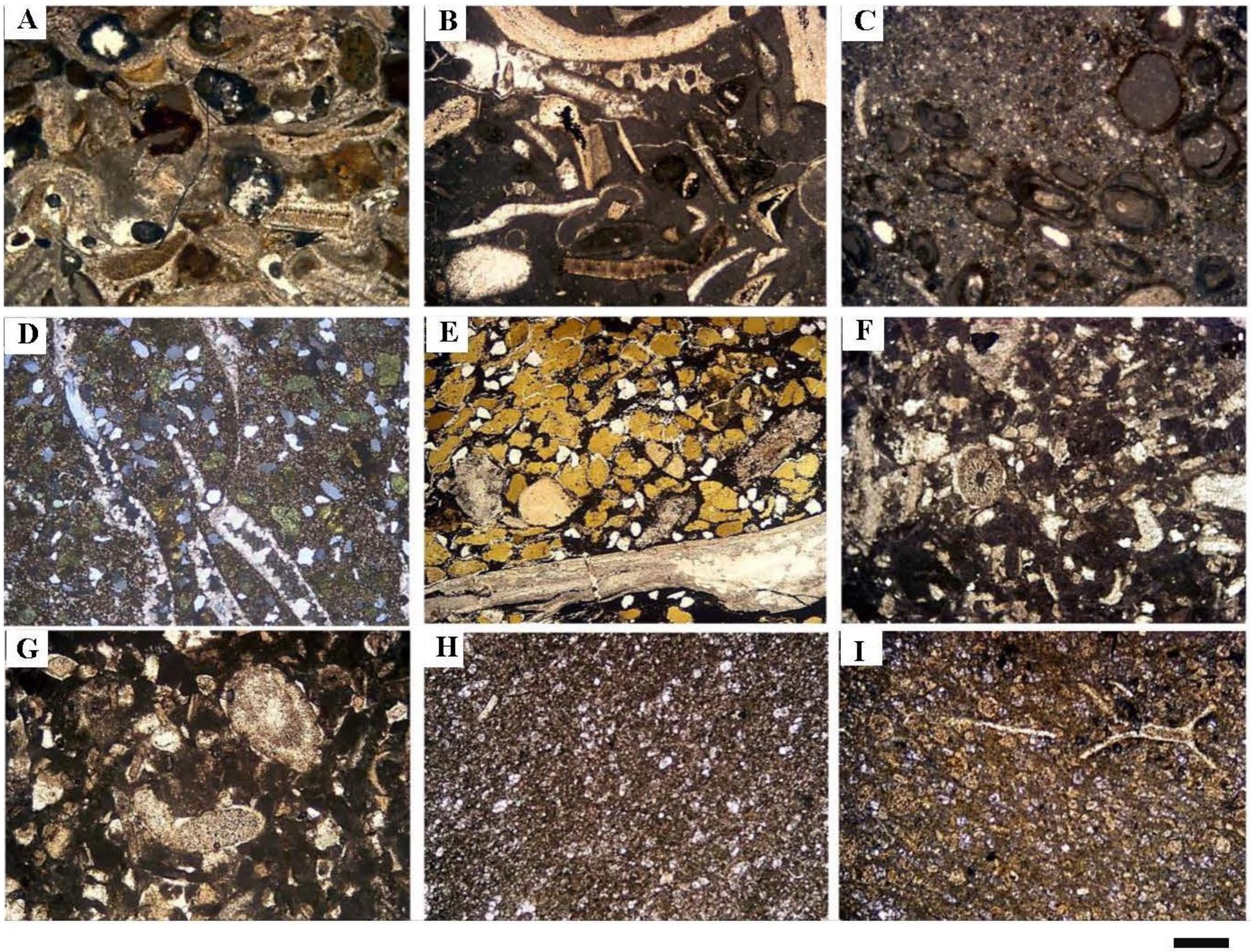

Fig. 13

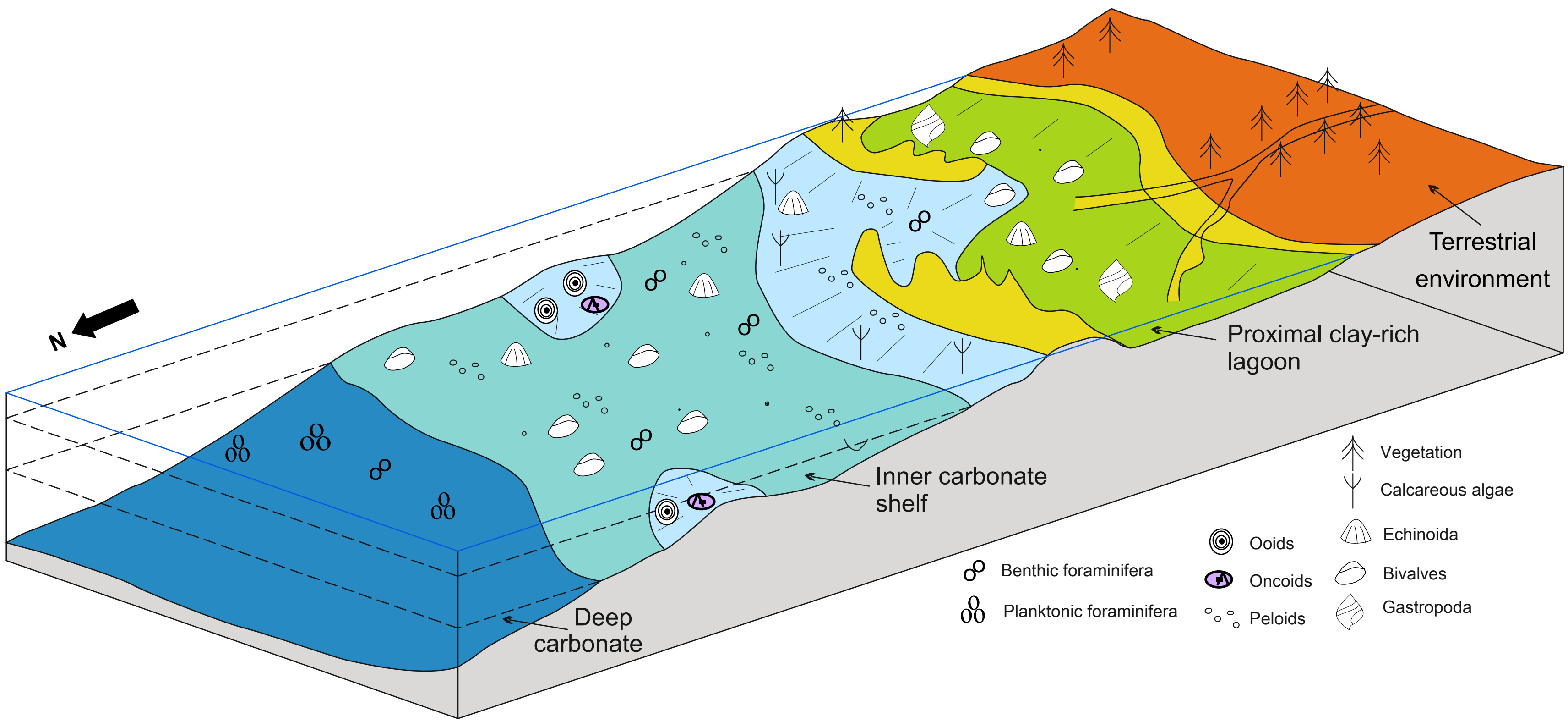
N
Terrestrial environment
Proximal clay-rich lagoon
Inner carbonate shelf
Deep carbonate
Vegetation
Calcareous algae
Echinoida
Bivalves
Gastropoda
Ooids
Oncoids
Peloids
Benthic foraminifera
Planktonic foraminifera

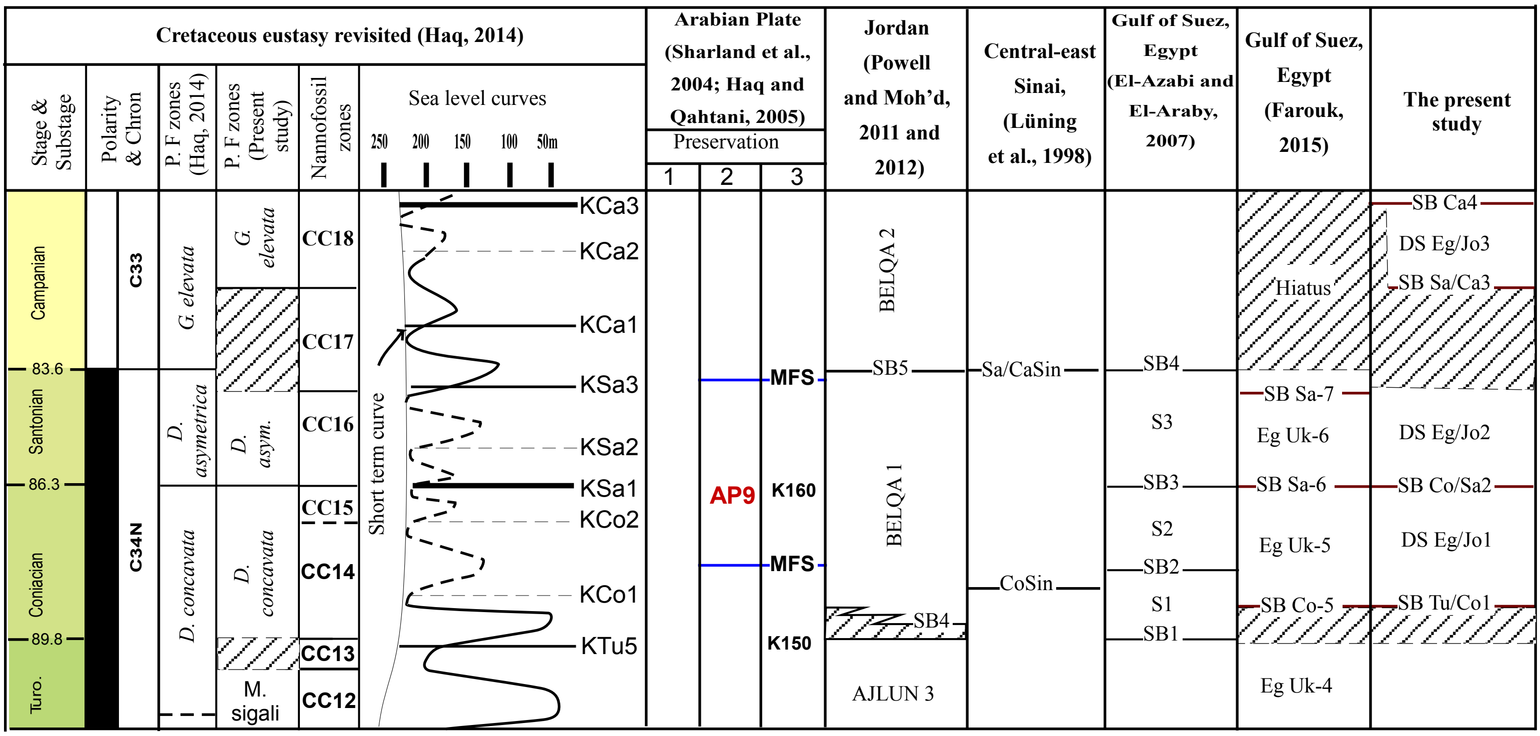

Cretaceous eustasy revisited (Haq, 2014)
Stage & Substage
Polarity & Chron
P. F zones (Haq, 2014)
P. F zones (Present study)
Nannofossil zones
Sea level curves
250 200 150 100 50m
Short term curve
Campanian
Santonian
Coniacian
Turo.
83.6
86.3
89.8
C33
C34N
G. elevata
D. asymetrica
D. concavata
D. asym.
M. sigali
CC18
CC17
CC16
CC15
CC14
CC13
CC12
KCa3
KCa2
KCa1
KSa3
KSa2
KSa1
KCo2
KCo1
KTu5
Arabian Plate (Sharland et al., 2004; Haq and Qahtani, 2005)
Preservation
1 2 3
MFS
AP9
K160
MFS
K150
Jordan (Powell and Moh'd, 2011 and 2012)
BELQA 2
SB5
BELQA 1
SB4
AJLUN 3
Central-east Sinai, (Lüning et al., 1998)
Sa/CaSin
CoSin
Gulf of Suez, Egypt (El-Azabi and El-Araby, 2007)
SB4
S3
SB3
S2
SB2
S1
SB1
Gulf of Suez, Egypt (Farouk, 2015)
Hiatus
SB Sa-7
Eg Uk-6
SB Sa-6
Eg Uk-5
SB Co-5
Eg Uk-4
The present study
SB Ca4
DS Eg/Jo3
SB Sa/Ca3
DS Eg/Jo2
SB Co/Sa2
DS Eg/Jo1
SB Tu/Co1

Fig. 15

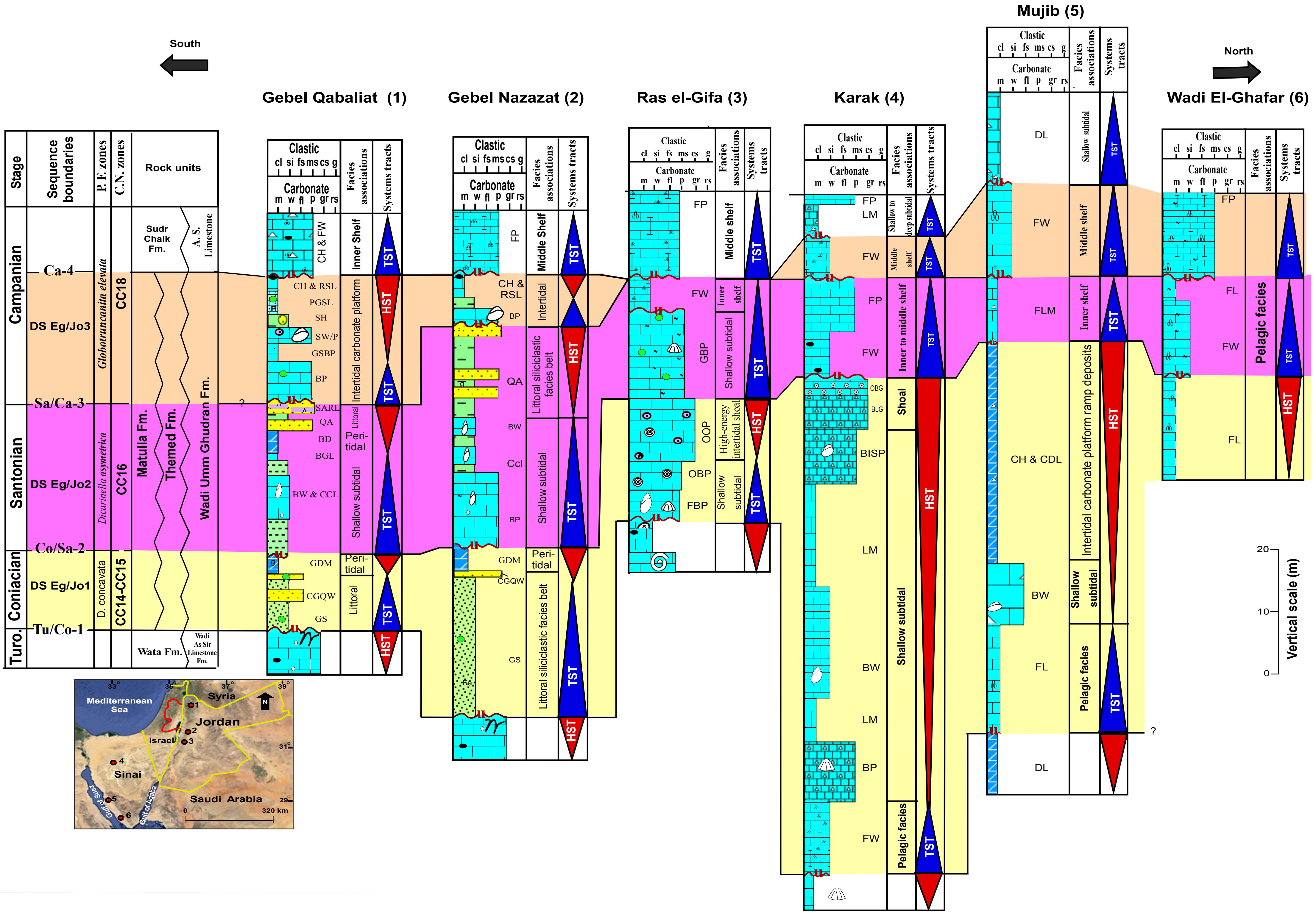
South
North
Gebel Qabaliat (1)
Gebel Nazazat (2)
Ras el-Gifa (3)
Karak (4)
Mujib (5)
Wadi El-Ghafar (6)
Stage
Sequence boundaries
P. F. zones
C.N. zones
Rock units
Campanian
Santonian
Coniacian
Turo.
Ca-4
Sa/Ca-3
Co/Sa-2
Tu/Co-1
DS Eg/Jo3
DS Eg/Jo2
DS Eg/Jo1
Globotruncanita elevata
Dicarinella asymetrica
D. concavata
CC18
CC16
CC14-CC15
Sudr Chalk Fm.
A. S. Limestone
Matulla Fm.
Themed Fm.
Wadi Umm Ghudran Fm.
Wata Fm.
Wadi As Sir Limestone Fm.
Clastic
cl si fs ms cs g
Carbonate
m w fl p gr rs
Facies associations
Systems tracts
TST
HST
Inner Shelf
Intertidal carbonate platform
Littoral
Peri-tidal
Shallow subtidal
Middle Shelf
Intertidal
Littoral siliciclastic facies belt
Middle shelf
Inner shelf
Shallow subtidal
High-energy intertidal shoal
Shallow to deep subtidal
Inner to middle shelf
Shoal
Pelagic facies
Shallow subtidal
Intertidal carbonate platform ramp deposits
Pelagic facies
CH & FW
CH & RSL
PGSL
SH
SW/P
GSBP
BP
SARL
QA
BD
BGL
BW & CCL
GDM
CGQW
GS
FP
CH & RSL
QA
BW
Ccl
GDM
CGQW
GS
Fe
FW
GBP
OOP
OBP
FBP
LM
FLM
OBG
BLG
BISP
BW
DL
CH & CDL
FL
Vertical scale (m)
20
10
0
Mediterranean Sea
Syria
Jordan
Israel
Sinai
Saudi Arabia
Gulf of Suez
Gulf of Aqaba
320 km

FA	FT	Name	Description	Depositional environments and remarks
Littoral siliciclastic facies belt	**1**	Glauconitic ferruginous siltstone with shale (GS)	Predominantly greyish siltstone and mudstone (shale) with yellowish glauconitic pellets.	Restricted lower intertidal regime, below the mean storm wave base. (McRae 1972; Wanas 2008).
	2	Calcareous glauconitic quartz arenite (CGQA)	Greyish, orange to brownish yellow, calcareous glauconitic quartz-wacke dominated by sub-angular to sub-rounded, ill-sorted quartz grains (40-60%) with many scattered glauconitic pellets, agglutinated or disseminated in a ferruginous mud; sparse bioclasts.(Fig. 12A).	Shallow marine environment close to the shoreline / beach-face, with quartz grains supplied either by rivers or erosion of the coastal zone (Pettijohn el al. 1987).
	3	Quartz arenite (QA)	Fine- to coarse-grained, quartz grains (about 80% of the rock) which are ill-sorted, elongated to spherical, and rarely polycrystalline. A few oxidized glauconite peloids are present (Fig. 12B).	Lower shoreface setting (El-Azabi and El-Araby 2007).
	4	Sandy evaporitic recrystallized lime-mudstone (SARL)	Quartz arenite with poorly sorted, medium to coarse monocrystalline quartz grains, cemented by anhydrite and gypsum comprising interlocking coarse granular and prismatic crystals. Some iron oxide coating is present (Fig. 12C).	Coastal marine setting, subsequently subjected to emergence that resulted in the removal of the iron oxides and cementation by evaporite minerals in the peritidal zone.
Peritidal carbonate facies belt	**5**	Ferruginous sandy dolomicrite (FSDM)	Dark lime mud, rich in well-defined, clear dolomitic rhombs containing some skeletal particles. Dolomite rhombs account for about 30-40% of the rock. Rare elongated molluscan shell fragments are present (Fig. 12D).	Restricted peritidal environment during denotes a fall in relative sea-level (LaMaskin and Elrick 1997; Warren 2000).
	6	Ferruginous glauconitic dolomicrite (FGDM)	Mainly very fine dolomite rhombs (70-80%) with skeletal particles, as well as abundant glauconitic pellets, the latter partially coated by finely crystalline calcite.	Fine crystalline dolomite is interpreted to be a result of early diagenetic alteration of micrite (lime-mud) in a shoaling, peritidal environment (Warren 2000; El-Azabi and El-Araby 2007).
Intertidal carbonate platform ramp deposits	**7**	Coarse dolomitic mudstone (CDM)	Coarse-grained crystalline carbonate rock dominated by dolomite crystals. Dolomite occurs as crystalline masses of subhedral to euhedral coarse dolomite rhombs (70-100µm).	Coarse crystalline dolomite is interpreted to be a result of late diagenetic alteration of micrite in a lower intertidal setting.
	8	Siliceous recrystallized lime-mudstone (SRL)	Skeletal grains make up less than 5% of the rock. It is mostly composed of micrite and microspar.	The lack of deep-water microfossils in the original lime-mud matrix, and the presence of biogenic silica indicates an intertidal environment.

	9	Recrystallized sandy dolomicrite (RSL)	Consists of a well-developed macrocrystalline calcite groundmass cementing medium- to fine-grained, monocrystalline subrounded to subangular grain-supported quartz (Fig. 12E).	Deposited in an intertidal environment.
	10	Phosphatic glauconitic sandy lime-mudstone (PGSL)	Phosphatised bioclastics with authigenic glauconite pellets and fine- to very fine quartz grains, closely packed in a dark, dense lime–mud matrix (Fig. 12F).	Near-shore depositional environment (Glenn and Arthur 1990).
	11	Ooidal bioclastic wacke/packstone (OBP)	The allochems are represented mainly by spherical to elliptical radially fibrous ooids and shelly bioclasts (mostly bivalves) (Fig. 12G).	Radiallly-fibrous ooids and bioclasts with a micritic matrix indicate deposition in a shallow-water, agitated tidal lagoon (Palma et al. 2005; Wanas 2008).
	12	Chert-bearing limestone (Ch)	Well-bedded, massive and nodular chert is recorded in the Upper Carbonate Member of the Matulla Formation and Tafilah Member of Wadi Umm Ghudran Formation, usually parallel to the bedding planes (Fig. 12H).	Cherts in the region are interpreted as occurring during early diagenesis of biogenic silica sols (Steinitz, 1981; Fink and Reches 1983; Powell and Moh'd 2012).
High-energy intertidal shoal	13	Serpulid bioclastic wacke/packstone;	Consists mainly of serpulid tubes with a sparry calcite cement centre. Low diversity echinoid and bivalve fragments are embedded in sparry calcite cement. Fine- to very fine quartz sand grains are present (Fig. 12I).	Deposited in a high-energy warm-water, intertidal shoal environment (Flügel 2004).
	14	Glauconitic peloidal packstone (GPP)	Coarse-grained bioclastic grainstone to packstone dominated by echinoid spines and bivalve/gastropod shell debris, embedded in a micrite cement (Figs. 13A).	Deposited in high-energy, intertidal sand shoals.
Shallow subtidal facies belt	15	Calcareous clay (Ccl)	Yellowish grey, massive, calcareous and partly glauconitic with sparse oysters and burrows. Some sparse authigenic sand nodules are interpreted as back-filled crustacean burrows (*Thalassinoides*). The carbonate cement (about 20%) is patchy.	Calcareous claystone resulting from suspension fall-out suggests a low energy marine environment in a restricted inner lagoon environment.
	16	Bioclastic glauconitic lime mudstone (BGL)	Glauconitic lime-mudstone with vary rare and low-diversity, smooth-shelled ostracods embedded in micritic matrix.	Restricted shallow subtidal environment.
	17	Bioclastic wackestone (BW)	Bioclastic wackestone containing poorly sorted, recrystallized bivalve shell fragments (20%) loosely packed in a dense and dark grey, fine-grained micritic matrix.	Subtidal environment with open marine circulation, slightly below storm wave-base, (Wilson 1975; Flügel 2004).

	18	Bioclastic packstone (BP)	Fine- to medium-grained bioclastic packstone dominated by randomly oriented recrystallized, molluscan fragments (25%;gastropods and bivalves), echinoid plates and spines (20%) (Fig. 13B).	Open shallow lagoon environment with moderate water energy.
	19	Foraminiferal bioclastic packstone (FBP)	Medium-grained, bioclastic peloidal packstone dominated by micritized foraminifera and molluscan bioclasts (10%), with minor intraclasts, within a micrite matrix. Peloids are rounded, irregularly shaped grains and frequently contain relict structures.	Elliptical voids in the matrix are interpreted to be burrows, and together with the micritized foraminifera and molluscan fragmentrs, indicate an oxygenated shoreface depositional environment.
	20	Sandy bioclastic packstone (SBP)	Disarticulated bivalve shells and echinoderms are the most abundant bioclasts. Minor foraminifera (mostly miliolids and rotalids), calcispheres and sponge spicules occur.	Abundant and diverse shelly fauna suggests deposition in a high-energy, sandy shoal environment, in a proximal platform setting.
	21	Oncoidal bioclastic packstone (OBP)	Oncoids are well-sorted and well-rounded with nuclei of mainly carbonate grains, encrusted with asymmetric laminae of thin and crinkly laminated algal micrite. Ostracodes of ovoid or lensoid shape are heavily micritized (Fig. 13C).	Oncoid formation suggests a periodically turbulent environment which caused overturning in shallow, low-energy environments (Tucker and Wright 1990; Flügel, 2004).
	22	Glauconitic sandy bioclastic wackestone (GSBP)	Consists mainly of shell debris (echinoid spines, bivalves and gastropods) (Fig. 13D).	Interpreted as being deposited as high-energy sand shoals.
	23	Oyster glauconitic floatstone (OGF)	Microscopically, the rock is composed of low diversity, large oyster shells (recrystallized to fibrous calcite) floating in a dense lime mud matrix with oxidized glauconite peloids. (Fig. 13E).	Deposited in a restricted, quiet water near-shore setting with low sedimentation rates.
	24	Bio – intraclastic sandy packstone (BISP)	Consists of peloids (30-40%), intraclasts (20-30%) and fossil fragments, especially echinoids, (10-15%), embedded in sparry calcite cement (Figs. 13F & G).	Shallow subtidal setting, with periodic,high-energy conditions (LaMaskin and Elrick 1997; Bachmann and Hirsch 2006).
Pelagic Facies	**25**	Foraminiferal lime-mudstone (FLM)	Composed of micrite with sparse foraminiferal tests; microspar calcite patches are the result of aggrading neomorphism. Some yellowish glauconitic pellets are also present.	Shallow inner neritic environment, in warm water, low-energy conditions.
	26	Foraminiferal wacke/packstone (FP)	Foraminiferal wacke/packstone dominated by variable planktonic foraminiferal bioclasts (80% of allochems) embedded in a lime-mud matrix (Figs. 13H & I).	Deposited in a deep-water marine environment , varying from deep-inner to middle-neritic palaeobathymetry.

Table 3: Facies types recognized in the present study.